Bioactive Materials 6 (2021) 191–207

Contents lists available at ScienceDirect

Bioactive Materials

journal homepage: http://www.keaipublishing.com/biomat

Synergistic effects of immunoregulation and osteoinduction of ds-block elements on titanium surface

Lan Chen[a,b], Donghui Wang[c], Jiajun Qiu[a], Xianming Zhang[a], Xingdan Liu[a,b], Yuqin Qiao[a,**], Xuanyong Liu[a,b,d,*]

[a] State Key Laboratory of High Performance Ceramics and Superfine Microstructure, Shanghai Institute of Ceramics, Chinese Academy of Sciences, Shanghai, 200050, China
[b] Center of Materials Science and Optoelectronics Engineering, University of Chinese Academy of Sciences, Beijing, 100049, China
[c] School of Materials Science and Engineering, Hebei University of Technology, Tianjin, 300130, China
[d] School of Chemistry and Materials Science, Hangzhou Institute for Advanced Study, University of Chinese Academy of Sciences, Hangzhou, 310024, China

ARTICLE INFO

Keywords:
Ds-block element
Valence electron
Immune response
Osteoimmunology
Molecular mechanism

ABSTRACT

Ds-block elements have been gaining increasing attention in the field of biomaterials modification, owing to their excellent biological properties, such as antibiosis, osteogenesis, etc. However, their function mechanisms are not well understood and conflicting conclusions were drawn by previous studies on this issue, which are mainly resulted from the inconsistent experimental conditions. In this work, three most widely used ds-block elements, copper, zinc, and silver were introduced on titanium substrate by plasma immersion ion implantation method to investigate the rule of ds-block elements in the immune responses. Results showed that the implanted samples could decrease the inflammatory responses compared with Ti sample. The trend of anti-inflammatory effects of macrophages on samples was in correlation with cellular ROS levels, which was induced by the implanted biomaterials and positively correlated with the number of valence electrons of ds-block elements. The co-culture experiments of macrophages and bone marrow mesenchymal stem cells showed that these two kinds of cells could enhance the anti-inflammation and osteogenesis of samples by the paracrine manner of PGE2. In general, in their steady states on titanium substrate (Cu^{2+}, Zn^{2+}, Ag), the ds-block elements with more valence electrons exhibit better anti-inflammatory and osteogenic effects. Moreover, molecular biology experiments indicate that the PGE2-related signaling pathway may contribute to the desired immunoregulation and osteoinduction capability of ds-block elements. These findings suggest a correlation between the number of valence electrons of ds-block elements and the relevant biological responses, which provides new insight into the selection of implanted ions and surface design of biomaterials.

1. Introduction

The elements with (n-1) $d^{10}ns^{1-2}$ valence electronic structures are termed as ds-block elements, which contain eight elements in the group IB and IIB. Due to their full d atomic orbital, ds-block elements are prone to coordinate with biomolecules and exhibit many physiological functions, thus, they are widely used in biomaterial fields [1–4]. There are two main applications of ds-block elements in the biomaterial field according to the previous work: directly used as the main component of the biomaterials (e.g. the gold neural probes, zinc cardiovascular stents, or internal fixation devices, etc.) or as dopants [5–9]. When ds-block elements are used as dopants, they have a wider range of applications and receive more attention in the biomaterial field, especially in the orthopedic implants filed [10–12].

Numerous studies have shown that introducing ds-block elements to the interior or surface of various biomaterials can endow the substrate with osteogenesis [9,13,14]. But the relevant mechanism is not clear and inconsistency exsits among different studies. This is two-fold: 1) Conclusions on the osteogenic action of a certain ds-block element from different studies are conflicting. For example, several studies have shown that the incorporation of Zn and Cu onto biomaterials could stimulate the osteogenic activity of mesenchymal stem cells, while,

Peer review under responsibility of KeAi Communications Co., Ltd.
* Corresponding author. State Key Laboratory of High Performance Ceramics and Superfine Microstructure, Shanghai Institute of Ceramics, Chinese Academy of Sciences, Shanghai, 200050, China.
** Corresponding author.
E-mail addresses: qiaoyq@mail.sic.ac.cn (Y. Qiao), xyliu@mail.sic.ac.cn (X. Liu).

https://doi.org/10.1016/j.bioactmat.2020.08.001
Received 8 July 2020; Received in revised form 1 August 2020; Accepted 1 August 2020

others have indicated that the supplementation of Zn and Cu would result in the inhibition of the osteogenic activity of rat bone marrow mesenchymal stem cells (rBMSCs) [8,15–18]. Also, there are similar research results of Ag and Au incorporated-biomaterials [19–22]. These contradictions may be mainly caused by the differences in the existing state, element content, and the experimental conditions of ds-block elements in various studies. 2) Inconsistent results exist between *in vitro* and *in vivo* experiments. For instance, the biomaterials introduced with ds-block elements, especially, Cu and Ag, exhibit the favorable antibacterial ability and osseointegration activity *in vitro* tests, while, some animal and clinical data report -the poor osseointegration around the implanted biomaterials [23–25]. The internal environment is much more complex than the simulation environment *in vitro*. It cannot be ignored that all biomaterials when implanted into the body trigger an immune response, which is the first step of tissue repair [26,27]. Therefore, it is necessary to consider the effects of implants on immune cells and the correlation between the bone cells and immune cells when evaluating the biomaterial-mediated osteogenesis *in vivo* [28,29].

To solve the above problems and uncover the real dependence of ds-block elements on the osteogenic activity, three elements, Zn, Cu, and Ag, were introduced onto the titanium surface by plasma immersion ion implantation (PIII) method in this work. Here, the PIII process is theoretically applicable to all elements in the periodic table. This method ensures that the different metal ions are uniformly distributed on the Ti substrate, making it possible to study the osteogenesis and immune response of different ds-block elements in the same condition [30,31]. Besides, the effects of different ds-block elements introduced samples on immunological and osteogenic activities were evaluated through *in vitro* and *in vivo* experiments by using RAW264.7 cells, mouse bone marrow mesenchymal stem cells (mBMSCs), and C57BL/6 mice. Meanwhile, mBMSCs were co-cultured with macrophages to mimic the environment *in vivo* to improve the reference value of *in vitro* results. Therefore, the results obtained from this study may provide a better guidance to the design and practical application of ds-block elements introduced biomaterials.

2. Materials and methods

2.1. Sample preparation

Titanium plates with the dimensions of 20 mm × 20 mm × 1 mm were used in the flow cytometry, the real-time polymerase chain reaction (RT-PCR) tests. The samples with dimensions of 20 mm × 10 mm × 1 mm were used in the zeta potential measurements and the sizes of samples used in other tests were 10 mm × 10 mm × 1 mm. All the samples were ultrasonically pretreated with a mixed acid solution (HF: HNO_3: H_2O = 1: 5: 4) to remove the oxide layers and ultrasonically cleaned successively with ethanol and distilled water (control group, denoted as Ti). Before plasma immersion ion implantation, the titanium plates were cleaned by radiofrequency argon ions for 15 min at a bias of 800 V in an argon atmosphere. Then, Zn, Cu, and Ag ions were implanted onto the pretreated titanium surface at 30 kV for 90 min (experiment groups, denoted as Zn-Ti, Cu-Ti, and Ag-Ti, respectively). The primary PIII parameters are listed in Table S1. During the ion implantation, the sample stage was cooled to about 25 °C by circulating water [32–35]. All samples were sterilized with 75% alcohol for 2 h before biological evaluation.

2.2. Characterizations

2.2.1. Surface structure and chemical characterization

The surface morphologies of samples were examined at 15 kV of accelerating voltage by field emission scanning electron microscopy (FE-SEM; Hitachi SU8220, Japan) and the surface roughness was measured by atomic force microscope in the tapping mode (AFM; Bruker Multimode 8 system, USA). The chemical compositions and chemical states of all samples were tested by X-ray photoelectron spectroscopy (XPS, Al target; PHI 5802, Physical Electronics Inc., Eden Prairie, MN, USA).

2.2.2. Assessments of ion release

The PIII samples were immersed in 5 mL phosphate buffer saline (PBS) at 37 °C for 1, 4, 7, 14, 21, and 28 d without stirring. At the end of each immersion time, the ion released solution was collected and stored at 4 °C, then, the fresh PBS was supplemented. The amounts of released metal ions (Zn, Cu, and Ag) were measured by inductively-coupled plasma optical emission spectrometry (ICP-OES; Nu Instruments, Wrexham, UK).

2.3. In vitro studies

2.3.1. Immunological evaluation

2.3.1.1. Macrophage culture. The mouse mononuclear-macrophage leukemia cells (RAW264.7; cells were kindly provided by Cell Bank of Chinese Academy of Sciences, Shanghai, China) were used to evaluate the effects of various samples on the behavior of immune cells. The culture process of macrophages was detailed in our previous study [36].

2.3.1.2. Cell proliferation and viability. AlamarBlue™ (Thermo Fisher Scientific Inc., USA) assay was used to measure the proliferation of macrophages on different samples. Briefly, cells with a density of 1×10^5 cells per well were seeded on samples (four replicates) and cultured for 4 h, 1 d, and 4 d. At the end of each incubation period, the samples were rinsed with 0.6 mL PBS to remove the unattached cells and incubation with 0.5 mL 10% alamarBlue™ (diluted with the fresh full medium) for 2 h at 37 °C in the dark. Then, 100 μL of the culture medium was transferred to a black 96-well plate to measure an excitation wavelength at 560 nm and an emission wavelength at 590 nm by using an enzyme labeling instrument (BioTek Cytation 5, USA).

2.3.1.3. Cell morphology. The cell morphologies on different samples were observed by SEM (accelerating voltage: 15 kV; S-3400 N TypeI, Hitachi, Japan). After incubation for 4 h, 1 d, and 4 d on samples, the cells were rinsed with PBS twice and fixed with 2.5% glutaraldehyde overnight at 4 °C in the dark. Then, cells were dehydrated sequentially in a series of ethanol solutions (30, 50, 75, 90, 95 and 100%, v/v) for 10 min and dried in the hexamethyl disilylamine/ethanol solution series (1: 2, 1: 1, 2: 1, and 1: 0).

2.3.1.4. Intracellular reactive oxygen species (ROS) test. The reactive oxygen species (ROS) assay kit was used to detect the intracellular ROS level. Macrophages were seeded on samples (five replicates) with a density of 1×10^5 cells per well on a 24-well cell plate. After cultured for 4 d, trypsin-EDTA (0.05%; Gibco, Thermo Fisher Scientific Inc., USA) was used to collect the cells on samples. Then, 2′, 7′-dichlorodihydrofluorescein diacetate (DCFH-DA) solution (Sigma-Aldrich, USA) was added and cultured with the collected cells for 30 min at 37 °C in the dark. Afterward, the cells were stained with 4′, 6-diamidino-2-phenylindole (DAPI) for 10 min at room temperature in the dark. An enzyme labeling instrument was used to detect the fluorescence intensity of 2′, 7′-dichlorofluorescein (DCF; excitation/emission wavelength: 488/525 nm), and DAPI (excitation/emission wavelength: 358/461 nm). The calculation of intracellular ROS level was F_{DCF}/F_{DAPI}, F_{DCF} and F_{DAPI} represent the fluorescence intensity of DCF and DPAI, respectively.

2.3.1.5. Immunofluorescence staining. The cells with a density of 1×10^5 cells per well were seeded on samples for 4 h, 1 d, and 4 d. After each incubation period, the cells were fixed with 4% paraformaldehyde (PFA) overnight at 4 °C, permeabilized with 0.1%

(v/v) Triton X-100 (Amresco, USA), and blocked Fc-receptor with 1 wt % bovine serum albumin (BSA; Sigma-Aldrich, USA). Next, the cells were incubated with the primary antibodies against-iNOS (1: 50; Novus, USA) and CD206 (1: 50; Abcam, UK) overnight at 4 °C in the dark. Then, the cells were incubated with the secondary antibodies donkey anti-rabbit IgG H&L Alexa Fluor 488 (1: 200; Invitrogen, Thermo Fisher Scientific Inc., USA) and donkey anti-mouse IgG H&L Alexa Fluor 594 (1: 200; Abcam, UK) for 2 h at room temperature. DAPI was used to stain the nuclei for 10 min in the dark. The confocal laser scanning microscope (Leica TCS SP8, Germany) was used to observe the immunofluorescence staining.

2.3.1.6. Flow cytometry. The expression levels of cell surface markers C-C chemokine receptor type 7 (CCR7, also known as CD197) and the cluster of differentiation 206 (CD206) were measured by flow cytometry. Macrophages with a density of 5×10^5 per well were seeded on samples on a 6-well plate for 4 d. Then, cells were collected by trypsin-EDTA (0.05%) and incubated with purified rat anti-mouse CD16/CD32 antibody (BD Pharmingen, USA) to block Fc-receptors for 10 min at room temperature. The detected cells were incubated with phycoerythrin (PE)-conjugated anti-mouse F4/80 antibody (BD Pharmingen, USA) and PE/Cy7-labeled anti-mouse CD197 (CCR7) antibody (Biolegend, USA) for 30 min at 4 °C in the dark. Next, the fixation/permeabilization solution (BD Pharmingen, USA) was added and incubated for 20 min at 4 °C. Then, the cells were incubated with allophycocyanin (APC)-conjugated anti-mouse CD206 antibody (BD Pharmingen, USA) for another 30 min at 4 °C. The cells were transferred to fluorescence activated cell sorting (FACS) tubes (0.5 mL per tube) to test by using BD LSRFortessa™ flow cytometer (Becton, Dickinson and Company, USA). 20,000 events per tube were analyzed by using FlowJo™ v10 software.

2.3.1.7. Enzyme-linked immunosorbent assay (ELISA). The cells with a density of 1×10^5 cells per well were seeded on samples on 24-well plates for 4 d. The cell culture medium was collected to detect the concentration of interleukin-1 receptor antagonist (IL-1ra; R&D System, USA), IL-4 (Anogen, Canada), IL-6 (Anogen, Canada), IL-10 (Raybiotech, USA), transforming growth factor-β (TGF-β; R&D System, USA) and tumor necrosis factor-α (TNF-α; Anogen, Canada) by ELISA. A microplate reader (Thermo Fisher Scientific Inc., USA) was used to detect the absorbance of the plate according to the protocol. The concentrations of the above-mentioned factors were calculated using standard curves.

2.3.1.8. Real-time polymerase chain reaction (RT-PCR) analysis. The immune-related gene expression levels were analyzed by RT-PCR test. Macrophages were seeded on samples on a 6-well plate with a density of 5×10^5 cells per well for 4 d. The total RNA was extracted using TRIzol™ reagent (Invitrogen, Thermo Fisher Scientific Inc., USA). Complementary DNA (cDNA) was synthesized from the total RNA using a transcriptor first-strand cDNA synthesis kit (Roche, Switzerland) according to the protocol. RT-PCR was conducted on the LightCycler® 480 system (Roche, Switzerland) using LightCycler® 480 SYBR Green I Master (Roche, Switzerland). House-keeping gene GAPDH was as the reference gene and the $2^{-\Delta\Delta Ct}$ analysis method was used to calculate the relative target gene expression levels [36]. The primers for RT-PCR were listed in Table S2 and all of the primers were purchased from BioTNT (Shanghai, China). RT-PCR experiments were performed at least twice and each sample was analyzed in triplicate. Relative expression was quantified using the comparative threshold method.

2.3.2. Osteogenic evaluation

2.3.2.1. Mouse bone marrow mesenchymal stem cells culture. The mouse bone marrow mesenchymal stem cells (mBMSCs; cells were kindly provided by Sciencell Biotechnology Co., Ltd, USA) were used to evaluate the osteogenic activity on different samples. The mBMSCs were cultured in DMEM medium (high glucose; Gibco, USA) with 15% fetal bovine serum (FBS; Gibco, USA) and 1% penicillin/streptomycin serum (antibiotic/antimycotic; Gibco, USA) on the cell culture flask in a humidified atmosphere of 5% CO_2 at 37 °C. Cells were passaged at a ratio of 1: 3 every three days. The primary mBMSCs used in the experiments were only passaged 2–4 times.

2.3.2.2. Cell adhesion and spreading assay. Cells with an initial density of 5×10^4 cells per well were seeded on samples in a 24-well plate. After cultured for 1, 4, and 24 h, the cells were fixed with 4% PFA overnight at 4 °C in the dark. Then, the cells were permeabilized with 0.1% (v/v) Triton X-100 for 2 min and 1% BSA were added to block Fc-receptor for 30 min. Next, the cells were stained with fluorescein isothiocyanate (FITC)-phalloidin (Sigma, USA) at room temperature for 1 h and stained with DAPI for another 5 min [37]. Cells were examined on a confocal laser scanning microscope.

2.3.2.3. Cell proliferation. Cells with a density of 1×10^4 cells per well were seeded on various samples (four replicates) and cultured for 1, 4, and 7 d. After each incubation period, a 10% alamarBlue™ solution was added to measure the cell proliferation as described in section 2.3.1.2.

2.3.2.4. Cell morphology. The cell morphology was observed by SEM. Cells were cultured on different samples with a density of 1×10^4 per well in a 24-well plate for 1, 4, and 7 d. After each incubation time, cells were fixed with 2.5% glutaraldehyde overnight at 4 °C and dehydrated sequentially as described in section 3.1.3.

2.3.2.5. Alkaline phosphatase (ALP) activity assay. The mBMSCs at a density of 7×10^3 cells per well were seeded on various samples (four replicates) on a 24-well plate and cultured for 10 d to measure the ALP activity [37]. First, cells were cracked for 40 min by using lysis buffer on the ice, the lysed cells were centrifuged at 8, 000 rpm for 10 min at 4 °C and collected. Next, *p*-nitrophenyl phosphate (pNPP) (Sigma-Aldrich, USA) was added to incubate for 30 min at 37 °C. Then, 1 M NaOH solution was added to terminate the reaction. The total ALP activity was calculated by measuring the absorbance at the wavelength of 405 nm with an enzyme labeling instrument and the total intracellular protein levels were quantified by using bicinchoninic acid (BCA) kit (Thermo Fisher Scientific Inc., USA). Finally, the ALP activity was normalized to the total protein content.

5-bromo-4-chloro-3-indolylphosphate/nitrobluetetrazoliumchloride (BCIP/NBT) alkaline phosphatase color development kit (Beyotime-Biotech Co., China) was used for ALP staining. After cultured for 10 d, cells were incubated with BCIP/NBT working solutions for more than 30 min in the dark and rinsed with ultrapure water twice. Stained cells were visualized by a fluorescence microscope (Olympus IX71, Japan).

2.3.2.6. Collagen secretion and extracellular matrix (ECM) mineralization assay. Collagen secretion and ECM mineralization on various samples were quantified by Sirius red (Sigma-Aldrich, USA) and alizarin red (Sigma-Aldrich, USA) staining, respectively [37]. Cells with a density of 7×10^3 cells per well were cultured on samples (four replicates) for 10 d. In collagen secretion assay, cells were fixed with 4% PFA for 20 min, and 0.1% Sirius red solution (dissolved in saturated picric acid) was added to stain for 18 h in the dark. Afterward, cells rinsed with 0.1 M acetic acid to remove the red dye, and images were taken by fluorescence microscopy. Eluent (0.5 mL per well; 0.2 M NaOH: methanol = 1: 1, v/v) was added to dissolve the stain and the absorbance of the stain at 540 nm was measured to quantify the collagen secretion. In ECM mineralization assay, cells were fixed with 75% ethanol solution for 1 h and stained with 40 mM alizarin red (pH = 4.2) for 10 min. Then, the cells were washed with distilled water to remove the excess red dye, and images were taken. Eluent (0.5 mL per well; 10% cetylpyridinium chloride dissolved in 10 mM sodium

phosphate, pH = 7) was added to dissolve the stain and the absorbance of the stain at 620 nm were measured to quantify the ECM mineralization.

2.3.2.7. RT-PCR analysis. The osteogenic gene expression levels were analyzed by RT-PCR test. Cells were seeded on samples on a 6-well plate with a density of 3×10^4 cells per well for 10 d. The total RNA was extracted using TRIzol™ reagent. The relevant protocol was by the method mentioned above. The primers for RT-PCR were listed in Table S3 and all of the primers were purchased from BioTNT. RT-PCR experiments were performed at least twice and each sample was analyzed in triplicate. Relative expression was quantified using the comparative threshold method.

2.3.3. Interactions between mBMSCs and the immune system

2.3.3.1. Macrophages and mBMSCs direct co-culture. Macrophages were seeded on various samples with a density of 1×10^5 cells per well on sample surfaces with the dimensions of 10 mm × 10 mm × 1 mm for 1 d and mBMSCs with a density of 7×10^3 per well were seeded on samples in the same dimensions for 7 d, respectively. Then, the samples, which had been seeded with macrophages and mBMSCs, were put in the same well to co-culture for another 3 d in a humidified atmosphere of 5% CO_2 at 37 °C. Similarly, macrophages with a density of 5×10^5 cells per well on samples with the dimensions of 20 mm × 20 mm × 1 mm for 1 d and mBMSCs with a density of 3×10^4 cells per well on samples in the same dimensions for 7 d. Next, the samples were also put in the same well to co-culture for another 3 d. In the co-culture condition, the two kinds of cells shared the same culture medium. The co-culture medium was also the DMEM medium with 15% FBS and 1% penicillin/streptomycin serum. After co-cultured for 3 d, the samples with macrophages and mBMSCs were separately removed onto new plates for biological evaluations. The schematic diagram of procedures for the co-culture experiment of macrophages and mBMSCs on the sample surface was shown in Fig. S1.

2.3.3.2. Immunological evaluation of co-cultured macrophages. After cultured for 1 d (cultured alone) and 4 d (co-cultured with mBMSCs), alamarBlue™ assay was used to measure the proliferation of macrophages cultured on the samples, the morphology of cells was observed by SEM and the immunofluorescence staining of macrophages was observed with a confocal laser scanning microscope. Also, after co-cultured with mBMSCs for 3 d, the immune responses of macrophages, including the ratio of M1 and M2 phenotype, the release of cytokines, and the immune-related genes expression levels, were analyzed by flow cytometry, ELISA, and RT-PCR tests, respectively. The detailed procedures of these assays were described in section 2.3.1.

2.3.3.3. Osteogenic evaluation of co-cultured mBMSCs. After cultured for 7 d (cultured alone) and 10 d (co-cultured with macrophages), the proliferation of mBMSCs was tested by alamarBlue™ assay, and the cell morphology was observed by SEM. The cell adhesion and spreading were measured by cytoskeletal staining with a confocal laser scanning microscope. Moreover, after co-cultured with macrophages for 3 d, ALP, collagen secretion, ECM mineralization, and RT-PCR assays were analyzed for osteogenic differentiation of mBMSCs. The detailed procedures of these assays were described in section 2.3.2.

2.3.3.4. PGE2-related signaling pathway in the co-culture experiment. The culture medium both in single-culture and co-culture conditions was collected to measure the total concentration of PGE2 (PGE2; Cayman Chemical, USA) released by macrophages and/or mBMSCs by ELISA. The PGE2-related gene expression levels of macrophages and mBMSCs were analyzed by RT-PCR tests. The primers for RT-PCR were listed in Table S4 and all of the primers were purchased from BioTNT. RT-PCR experiments were performed at least twice and each sample was analyzed in triplicate.

2.4. In vivo studies

2.4.1. Mouse air-pouch model

Six-week-old male pathogen-free C57BL/6 mice were maintained under specific pathogen-free conditions at the animal care facility in Shanghai Rat & Mouse Biotech Co., Ltd. The mouse air-pouch model was described previously [38,39]. Briefly, 4 mL of sterile air was injected subcutaneously into the lower dorsal area of mice to form an air pouch and a second injection of 3 mL of sterile air was performed four days later to reinforce the air pouch. Mice were anesthetized 48 h later by intraperitoneal injection of 1% pentobarbital sodium (1 mL per 100 g body weight) and the skin over the air-pouch was shaved thoroughly. Under the sterile condition, a surgical incision was made, one sample was implanted in each mouse.

2.4.2. Air-pouch tissues

The tissues were recovered from the mouse air-pouches 1 and 4 d after implantation. The air-pouch tissues were fixed in 4% PFA for histological analysis.

2.4.3. Histological analysis of air-pouch tissues

The air-pouch tissues were embedded in paraffin wax and sectioned to 4 μm. After dewaxing and dehydration, sections were stained with hematoxylin-eosin (HE) and Masson's trichrome. Stained sections were visualized by optical microscopy. ImageJ software was used to evaluate fibrous capsule thickness and the number of infiltrating cells in four random locations.

2.5. Statistical analysis

GraphPad Prism 6.0 (GraphPad Software, La Jolla, CA, USA) was used for statistical analysis. Quantitative data are expressed as mean ± standard deviation (SD). Statistically significant differences (p) were analyzed by one-way analysis of variance (ANOVA), two-way ANOVA, and Tukey's multiple comparison tests. A value of $p < 0.05$ was considered statically significant and was represented by the symbol "*", a value of $p < 0.01$ was represented by "**" and $p < 0.001$ was "***".

3. Results

3.1. Surface characterization

The surface characterization, including surface morphology, roughness, and chemical composition of all samples and ion release of the PIII samples (Zn-Ti, Cu-Ti, and Ag-Ti) were shown in Fig. 1. The acid etched Ti before ion implantation showed a flat surface with a micro-scale fluctuation topography (Fig. 1a). During ion implantation, the original micro-structure on the Ti surface was destroyed. A large number of silver nanoparticles (Ag NPs) of 30–50 nm in diameter were uniformly distributed on the Ag-Ti sample surface, while there were no any copper or zinc nanoparticles appearing on Cu-Ti and Zn-Ti sample surfaces, which are consistent with our previous works (Fig. 1a) [33–35]. It is possible that copper or zinc deposites on the titanium surface and easilyforms a stable copper/zinc-containing oxide layer which binds firmly to the substrate during the Cu/Zn ion implantation, while Ag NPs locally nucleates from the solid solution of α-Ti (Ag) to form metal particles on and below the titanium surface during the silver ion implantation [34,40,41]. Meanwhile, the surface roughness of PIII samples decreased, the Ti sample possessed the largest mean roughness (Ra) and root-mean-square height data (Rq) values compared with PIII samples (Fig. 1b). The values of Ra and Rq of Ti, Zn-Ti, Cu-Ti, and Ag-Ti samples were 53.7 nm and 65.4 nm, 40.0 nm and 50.9 nm, 42.8 nm and 54.1 nm, 22.9 nm and 39.2 nm, respectively. The maximum fluctuation heights of PIII samples also decreased. These results were consistent with SEM images.

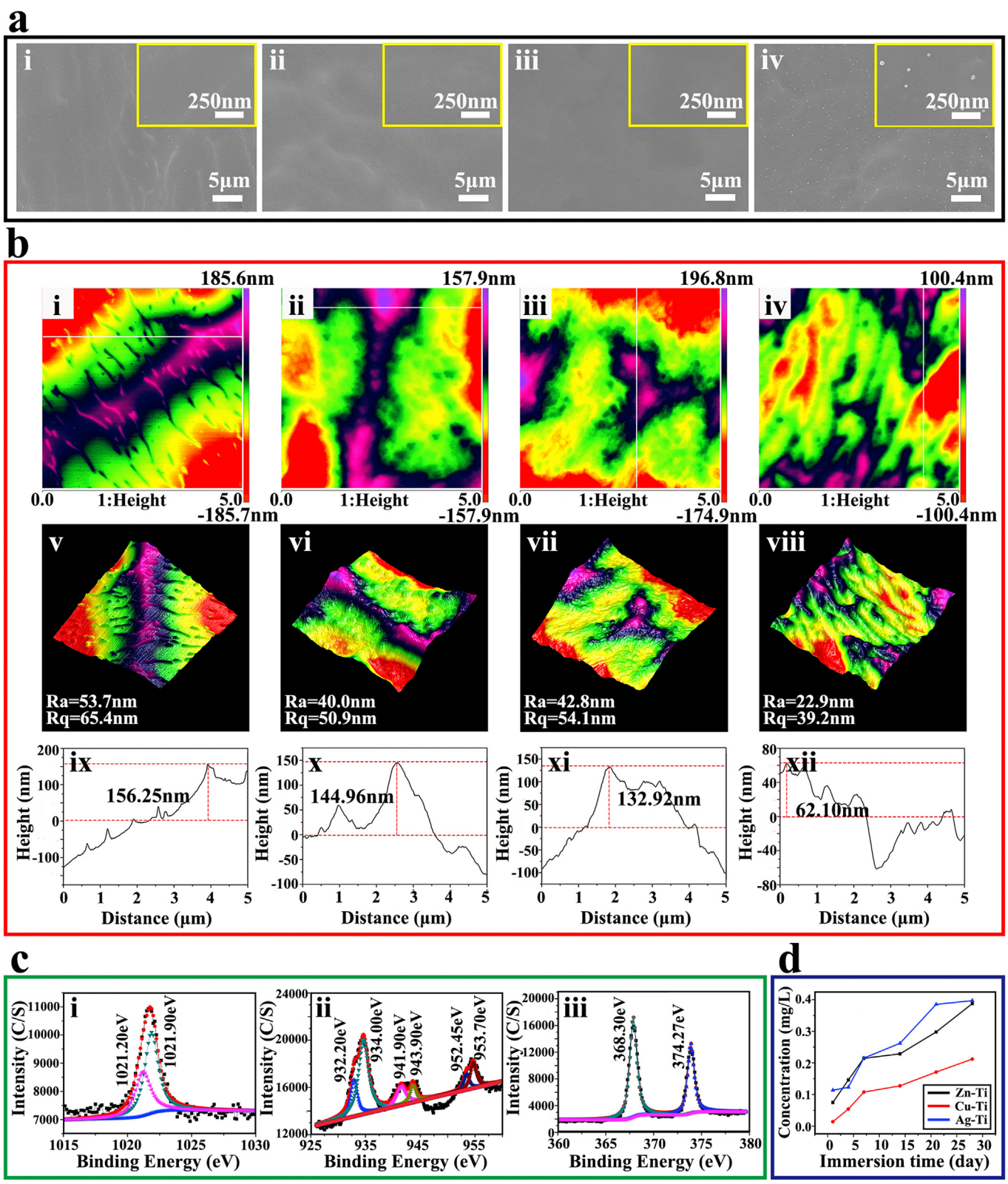

Fig. 1. Surface characterizations of various samples. (a) SEM images of the surface morphologies of various samples at low and high magnifications (i, ii, ii, and iv present Ti, Zn-Ti, Cu-Ti, and Ag-Ti, respectively). (b) AFM images of (i, ii, ii, and iv) two-dimensional morphologies, (v, vi, vii, and vii) three-dimensional morphologies, and (ix, x, xi, and xii) the depth profiles of different samples (i, v, and ix present Ti; ii, vi, and x present Zn-Ti; ii, vii and xi present Cu-Ti; iv, vii and xii present Ag-Ti). (c) XPS spectra of the Zn-Ti, Cu-Ti, and Ag-Ti samples. (d) The concentrations of implanted ions in PBS solution after immersion for 1, 4, 7, 14, 21, and 28 d.

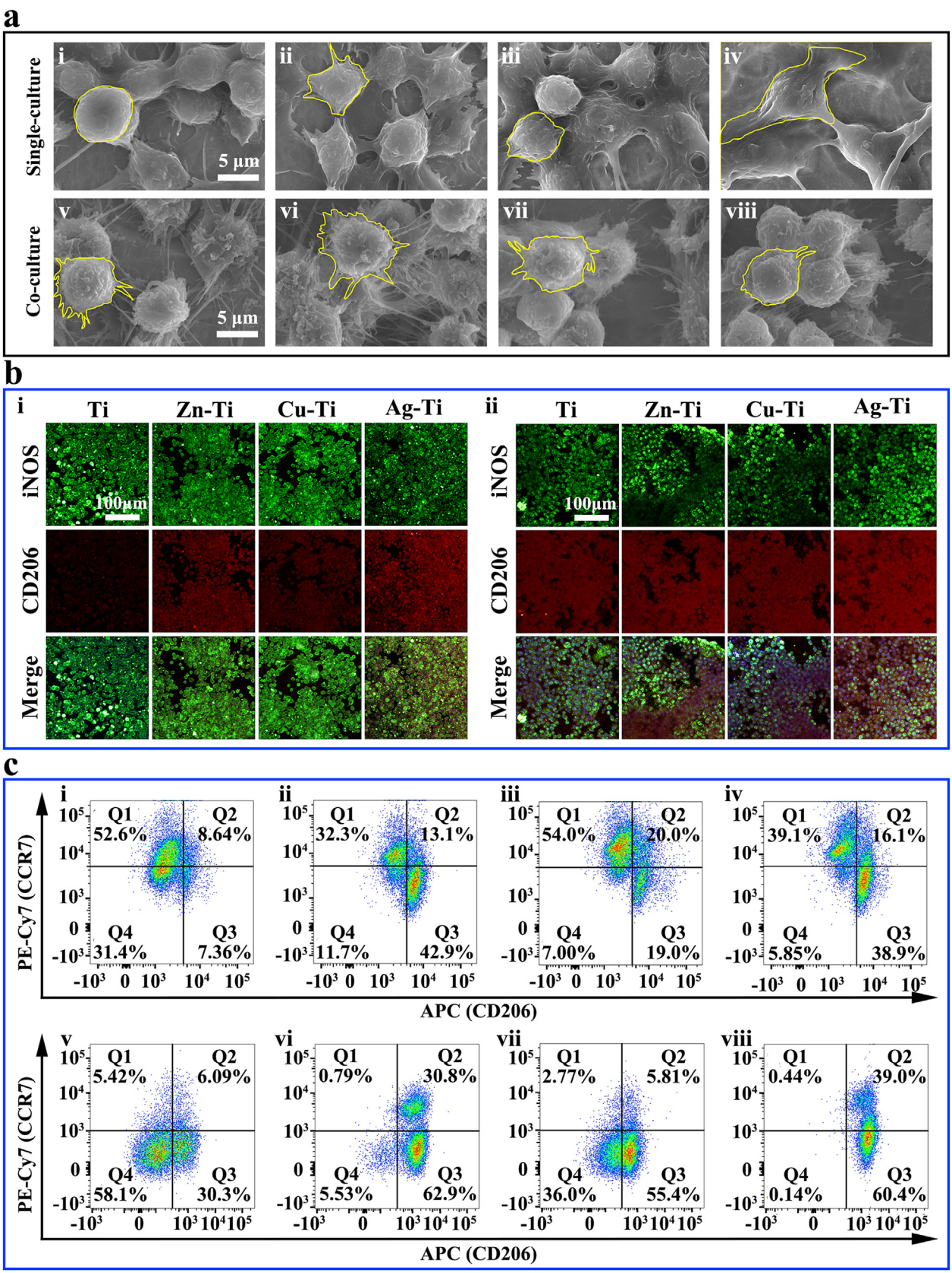

Fig. 2. Morphologies and polarization of macrophages on various samples *in vitro*. (a) SEM morphologies of macrophages in single-culture condition (i, ii, iii, and iv) and co-culture condition (v, vi, vii, and viii) after cultured for 4 d on samples at high magnifications (i and v present Ti; ii and vi present Zn-Ti; iii and vii present Cu-Ti; iv and viii present Ag-Ti). (b) Immunofluorescent staining images of macrophages in single-culture condition (i) and co-culture condition (ii) on various samples after cultured for 4 d; iNOS (green) was selected as M1 macrophage marker, CD206 (red) was selected as M2 macrophage marker, nuclei were stained with DAPI (blue). (c) Flow cytometry analyses of cell-surface markers on macrophages in single-culture condition (i, ii, iii, and iv) and co-culture condition (v, vi, vii, and viii) (i and v present Ti; ii and vi present Zn-Ti; iii and vii present Cu-Ti; iv and viii present Ag-Ti).

To determine the chemical composition and chemical states, all samples were analyzed by XPS. The XPS spectra of all samples were shown in Fig. S2 and the high-resolution spectral results of the PIII sample surface were shown in Fig. 1c. For the Zn-Ti sample, the Zn 2p peaks at 1021.20 eV and 1021.90 eV corresponded to the binding energy of zinc oxide (ZnO) [33,42]. There were six peaks in the high-resolution spectrum of Cu 2p on the surface of the Cu-Ti sample. The two peaks located at 932.20 eV and 952.45 eV corresponded to the binding energy of Cu 2p1/2 and Cu 2p3/2 in metallic Cu. The peaks at 934.00 eV and 953.70 eV accounted for the binding energy of Cu 2p1/2 and Cu 2p3/2 in CuO [35,43]. Also, there were two peaks at 941.90 eV and 943.00 eV on the Cu-Ti sample surface, which corresponded to the satellite peaks of Cu 2p3/2 in CuO [44]. The Ag 3d doublet peaks near 374.27 eV (Ag 3d3/2) and 368.30 eV (Ag 3d5/2) corresponded to metallic Ag and the peak of silver oxide was not detected on the surface of the Ag-Ti sample [34,45]. The quantitative results of the corresponding element content tested by XPS on various sample surfaces are shown in Table S5. The contents of the implanted ions on the surface of PIII samples were very close, about 2% of the total element content. The contents of the O element, which was in the form of TiO_2, on the Ag-Ti sample were lower than that on Zn-Ti and Cu-Ti samples, which were 39.65%, 44.33%, and 43.41%, respectively, while the contents of Ti on PIII samples were the same. These results also indicated that some of the zinc and copper on Ti surfaces were in the form of oxides (ZnO and CuO), while silver was only in the form of metallic Ag, which were consistent with the results of the high-resolution spectrum.

Because the high concentration of metal ions possessed cytotoxicity [46,47], the release of metal ions from PIII samples in PBS for 28 d was measured by ICP-OES, and the concentrations of released ions from PIII samples were presented in Fig. 1d. PBS was closer to the physiological environment than H_2O and saline solution in this work. The concentrations of implanted ions were slowly increased with the extension of immersion time and the amounts of released ions on PIII samples were very similar and in the same order of magnitude ($\sim 10^{-1}$ ppm). Additionally, copper and zinc exist as metallic ions (Cu^{2+}, Zn^{2+}) in PBS solution, while silver tends to combine with anions in PBS, such as chloride ions, and form precipitation. The other physical and chemical properties, such as water contact angle, zeta potential, and corrosion resistance, were shown in Figs. S3–S5 and Table S6. The introduction of ds-block elements showed no significant effects on the water contact angle of the titanium surface (Fig. S3). While, the introduction of different ds-block elements did significantly affect the electrochemical properties of the sample surface, including zeta potential and corrosion resistance (Figs. S4 and S5).

3.2. Immunological evaluation

Macrophages were seeded on sample surfaces and cultured alone to investigate the immune responses. Meanwhile, macrophages were co-cultured with mBMSCs to evaluate the effect of mBMSCs on the immune response of macrophages after implantation.

The proliferation of macrophages on PIII samples was not inhibited compared with that of cells on the Ti sample (Figs. S6 and S7). The cell proliferation on sample surfaces in the co-culture condition was consistent with those of macrophages cultured alone, indicating that mBMSCs did not adversely affect the proliferation of macrophages (Figs. S6 and S7). However, the morphologies of macrophages cultured alone on various samples were different. A small number of cells adhered to sample surfaces when cultured for 4 h and the cell number increased significantly after 1 d. Most of the cells were ellipsoid on all samples, while there were cells on the Ag-Ti sample with long filopodia (Fig. S8). When cultured for 4 d, macrophages grew in multiple layers on the sample surface. Cells were round on the Ti sample, but they resembled polygonal stars on the surfaces of Cu-Ti and Zn-Ti samples, cells were still spindle-shaped on the Ag-Ti sample. The different cell morphologies indicated that various samples had different influences on the adhesion and spread of macrophages (Fig. 2a and Fig. S9). The cell morphologies of macrophages in co-culture conditions were significantly different from those of macrophages cultured alone. All of the co-cultured macrophages grew in clusters on all sample surfaces and became round with a large number of filopodia (Fig. 2a), revealing that the addition of mBMSCs would alter the immune response of macrophages and this regulation might be stronger than the ds-block element's effect on immune cells.

CD206 (red; M2 macrophages) and iNOS (green; M1 macrophages) were selected for immunofluorescence staining assay to observe the polarization of macrophages on the sample surface (Figs. 2b and S10) [48,49]. The number of macrophages increased with the extension of the culture time, which was in accordance with the SEM results. The red fluorescence intensity of macrophages after cultured for 4 h and 1 d on the Ag-Ti sample was always the strongest ($p < 0.001$), while the green fluorescence intensity of macrophages on the Ti sample was the strongest ($p < 0.001$) among all groups (Fig. S10). When macrophages were cultured alone on sample surface for 4 d, a large number of macrophages were growing on the sample surfaces. The trend of red fluorescence intensity of cells on the sample surface was as follows: Zn-Ti > Ag-Ti > Cu-Ti > Ti (Figs. 2b and S10), which indicated that Ag-Ti and Zn-Ti samples could significantly stimulate the polarization of M2 macrophages and the regulation of Cu-Ti sample on macrophages was similar to that of Ti sample. When macrophages were co-cultured with mBMSCs, the green fluorescence intensity of macrophages on Ti sample increased, while, that of cells on PIII samples decreased. The red fluorescence intensity of the co-cultured macrophages on all samples became stronger than those of macrophages cultured alone (Figs. 2b and S10). These results indicated that the addition of mBMSCs could promote macrophages on PIII samples to polarize into the M2 phenotype rather than the M1 phenotype.

Flow cytometry was used to quantitatively analyze the proportion of M1 and M2 phenotype macrophages cultured on sample surfaces. F4/80 was selected as the marker of macrophage, CCR7 was chosen as the marker of M1 macrophage, and CD206 was selected as the marker of M2 macrophage [39,50]. The analyzed macrophages on the sample surface were located in the region P2 ($F4/80^+$) (Fig. S11). As shown in Fig. 2c, the $F4/80^+$ macrophages polarized under the stimulation of samples and were divided into three groups, located in regions Q1 ($CCR7^+/CD206^-$; M1 macrophages), Q3 ($CCR7^-/CD206^+$; M2 macrophages) and Q4 ($CCR7^-/CD206^-$; M0 macrophages), and a small number of cells located in region Q2 ($CCR7^+/CD206^+$; M1/M2 macrophages). The proportion of polarized macrophages on PIII samples, including M1 and M2 macrophages, was significantly higher compared with that of cells on the Ti sample. The proportion of M2 macrophages cultured alone showed the following trend: Zn-Ti > Ag-Ti > Cu-Ti > Ti. Conversely, the trend of M1 macrophages' proportion was: Cu-Ti > Ti > Ag-Ti > Zn-Ti (Fig. 2c). When macrophages were co-cultured with mBMSCs, the ratio of M2 macrophages on all samples notably increased, while the proportion of M1 macrophages decreased. The trend of M2 macrophages' ratio was Zn-Ti > Ag-Ti > Cu-Ti > Ti. The results showed that the introduction of ds-block elements could promote the polarization of macrophages, especially Ag-Ti and Zn-Ti samples could promote the polarization of M2 phenotype macrophages. Moreover, adding mBMSCs could enhance macrophages on PIII sample surfaces to polarize into the M2 phenotype, which was consistent with the results of immunofluorescence staining.

All cells can release a variety of cytokines, which would affect their functions through an autocrine manner or affect the physiological functions of surrounding cells through paracrine manner [51,52]. The concentration of released cytokines of macrophages both in single-culture and co-culture conditions was measured by ELISA assay (Fig. 3a). When macrophages were cultured alone for 4 d, the amounts of pro-inflammation cytokine IL-6 and TNF-α released by cells on Zn-Ti and Cu-Ti samples were slightly lower than that of cells on Ti and Ag-Ti samples. There was no significant difference in the amounts of the anti-

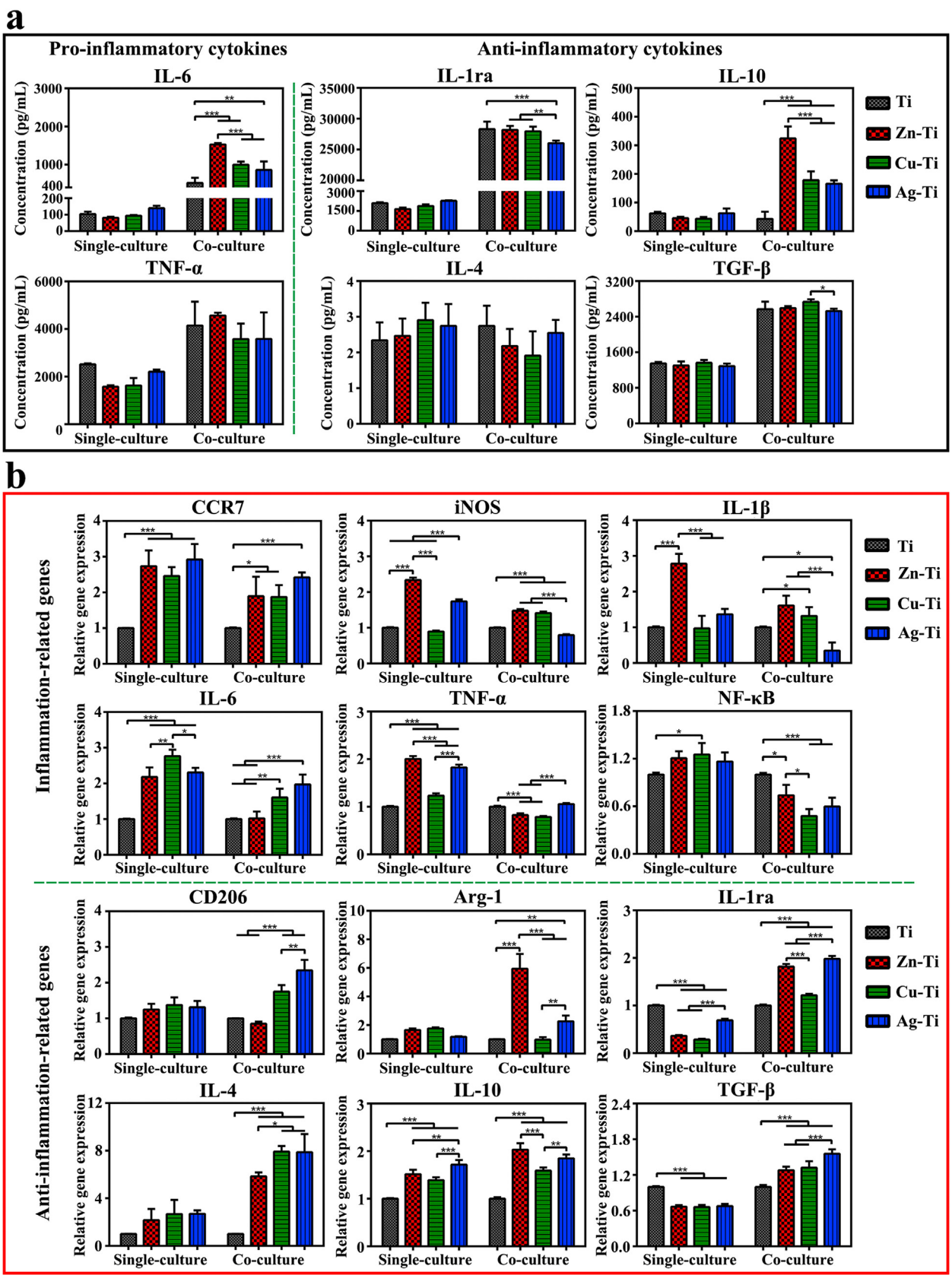

Fig. 3. Immune responses of macrophages on various samples *in vitro*. (a) ELISA determination of cytokines secreted from macrophages in single-culture and co-culture conditions after incubation on samples for 4 d. (b) Relative mRNA expression levels of the immune-related genes in macrophages in single-culture and co-culture conditions on day 4 after cultured on sample surfaces.

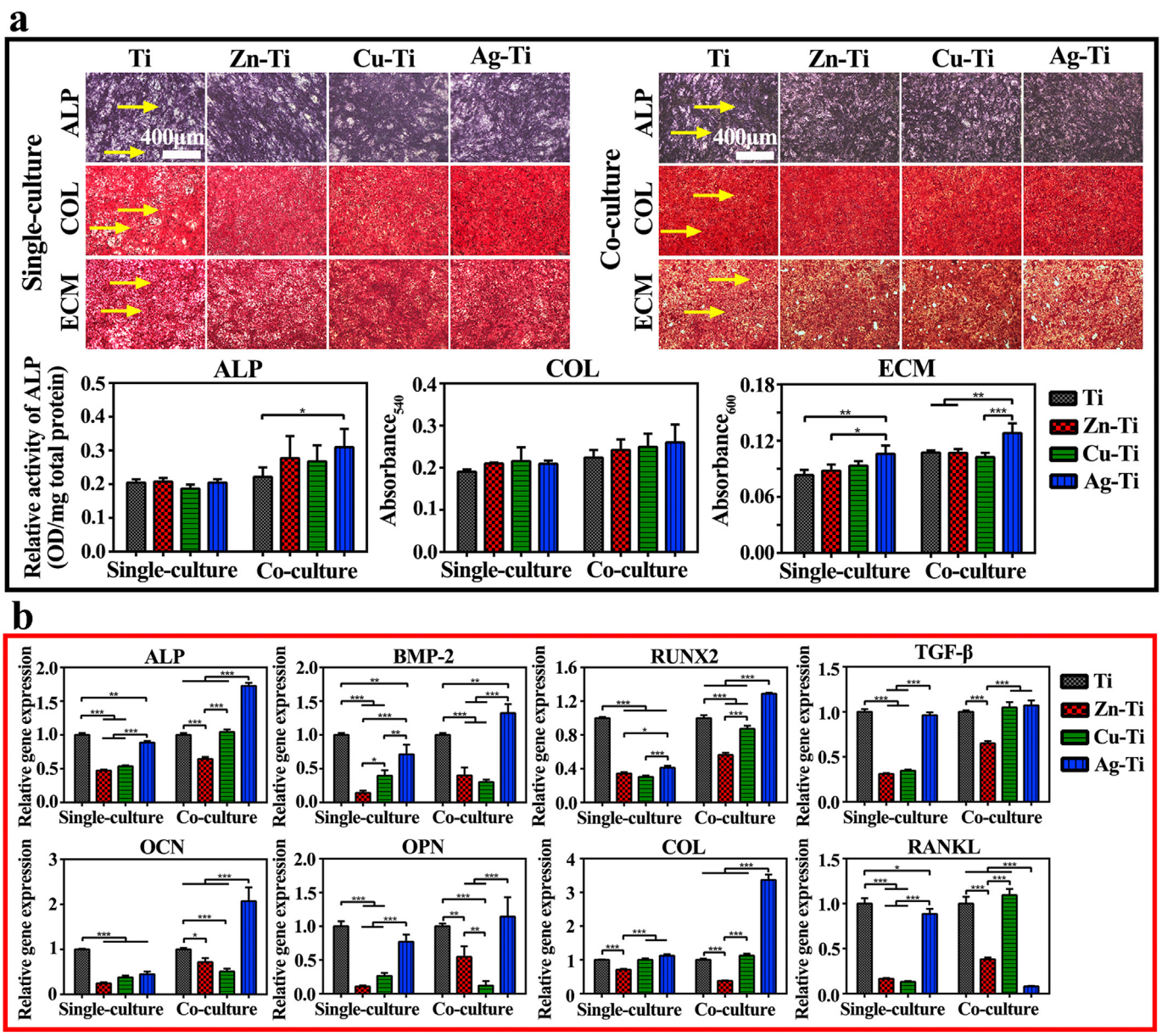

Fig. 4. Osteogenic activity of mBMSCs on various samples *in vitro*. (a) ALP positive areas, collagen secretion, and extracellular matrix mineralization of mBMSCs cultured on various samples for 10 d in single-culture and co-culture conditions and the corresponding colorimetrically qualitative results. (b) Relative mRNA expression levels of the bone formation-related genes in mBMSCs in single-culture and co-culture conditions on day 10 on sample surfaces.

inflammatory cytokines (IL-1ra, IL-4, IL-10, and TGF-β) released by cells on all samples. When macrophages were co-cultured with mBMSCs, the amounts of all released cytokines in the cell culture medium increased. The amounts of IL-6 and TNF-α released by cells on the Zn-Ti sample became the highest, while the amount of IL-6 released by cells on Ti was the lowest. There was no difference in the amounts of TNF-α released by cells on the other three samples. The amounts of IL-10 released by cells on PIII samples were higher than that of cells on Ti samples and that of cells on the Zn-Ti sample was the highest among PIII samples. The amounts of IL-4 released by macrophages on Ag-Ti samples were highest among PIII samples. There was no significant difference in the amounts of TGF-β cytokine of co-cultured macrophages among all samples. It was possible that mBMSCs could promote the polarization of macrophages so that the amounts of immune cytokines released by macrophages co-cultured with mBMSCs increased. The results of ELISA assays were accordant with the results of flow cytometry.

The immune-related gene expression levels were analyzed by RT-PCR tests (Fig. 3b). All PIII samples could stimulate the polarization of macrophages, the expression level of pro-inflammatory and anti-inflammatory genes (except IL-1ra and TGF-β) of macrophages on PIII samples increased compared with those of cells on the Ti sample. When macrophages were cultured alone, the expression levels of inflammation-related genes (CCR7, iNOS, IL-1β, and TNF-α) of macrophages on the Zn-Ti sample were the highest among these of cells on all PIII samples and were about 2-times higher than those of cells on Ti sample. The expression levels of CCR7, iNOS, IL-6, and TNF-α genes of cells on the Ag-Ti sample were more than 2-times higher than those of cells on the Ti sample. The expression levels of anti-inflammation-related genes (CD206, arginase-1 (Arg-1), IL-4, and IL-10) of cells on PIII samples were similar but were higher than those of cells on the Ti sample. And most of the immune-related genes expression levels of cells on the Cu-Ti sample were lower than those of cells on Zn-Ti and Ag-Ti samples. When macrophages were co-cultured with mBMSCs, the expression levels of inflammation-related genes of macrophages on PIII samples decreased, while the expression levels of anti-inflammatory genes of

cells on the PIII sample surface significantly increased compared with that of cells on the Ti sample. Especially, the expression levels of pro-inflammatory genes (iNOS, IL-1β, and NF-κB) of cells on the Ag-Ti sample decreased to half of the expression levels of cells on the Ti sample. The gene expression levels of iNOS, IL-6, IL-1β, and NF-κB of macrophages on the Zn-Ti sample decreased to the same level as those of cells on the Ti sample. While, the expression levels of anti-inflammatory genes of cells on the PIII samples became more than 2-times higher than that of cells on the Ti sample, especially, those of cells on Ag-Ti and Zn-Ti samples. It was possible that the obvious increase of anti-inflammatory gene expression levels of macrophages in co-culture conditions on sample surfaces, especially, Zn-Ti and Ag-Ti samples, resulted from that the polarization of M2 macrophages, which were promoted by mBMSCs (Fig. 2b and c). The PCR results were not completely consistent with the results of ELISA. Because PCR was used to test the expression level of mRNA in macrophages on the fourth day, while ELISA was used to test the expression level of protein released by cells within 4 d. The expression level of a protein over a few days was not the same. Moreover, many factors could affect the transcription and translation processes [53,54]. Thus, it was reasonable that the ELISA results do not coincide with the PCR results.

3.3. Osteogenic evaluation

The mBMSCs were cultured on the sample surfaces to evaluate the osteogenic activity and co-cultured with macrophages to observe the effects of immune responses on osteogenic activity (osteoimmunomodulation) [28]. Fig. S12 showed that PIII samples did not show any cytotoxicity to mBMSCs compared with titanium in single-culture and co-culture conditions. The mBMSCs on sample surfaces were found to be well spread with a variety of long filopodia and lamellipodia from SEM images and cytoskeletal staining results (Figs. S13 and S14).

The mBMSCs were stained by ALP staining kit, Sirius red, and alizarin red dye to analyze the osteogenic differentiation of cells on various samples in single-culture and co-culture conditions. The quantitative and qualitative staining results of ALP expression, collagen secretion, and ECM mineralization of mBMSCs were shown in Fig. 4a. The purple areas present intracellular ALP (the yellow arrows) and there was no significant difference in ALP staining results of mBMSCs in single-culture and co-culture conditions on Ti sample and PIII samples. ALP quantitative results revealed that the introduction of ds-block elements did not significantly enhance the osteogenic activity of mBMSCs cultured alone compared with the Ti sample, while the Ag-Ti sample slightly enhanced ALP generation in co-cultured mBMSCs. The reddish-brown areas represent the collagen secretion of mBMSCs on the sample surfaces. The staining results of collagen in mBMSCs both in single-culture and co-culture conditions on the four group samples were similar and there was no difference in collagen secretion of cells at the same culture condition on various samples. The yellow arrows show calcium nodules formation marked by alizarin red in ECM mineralization assay. According to the staining and quantitative results, the Ag-Ti sample could significantly promote ECM mineralization and calcium nodule formation compared with Ti and Zn-Ti samples. Besides, macrophages significantly enhanced the promotion of the Ag-Ti sample on ECM mineralization of mBMSCs ($p < 0.05$). These results showed that the Ag-Ti sample could significantly promote osteogenic differentiation of mBMSCs in the co-culture condition among the four groups.

The osteogenesis-related gene expression levels of mBMSCs on sample surfaces were displayed in Fig. 4b. When mBMSCs were cultured alone, the expression levels of osteogenic genes in mBMSCs on PIII samples were lower than those in mBMSCs on the Ti sample. In co-culture conditions, all of the osteogenic gene expression levels of mBMSCs on the Ag-Ti sample were statistically up-regulated among the four groups and were about 1.5-times to 2-times higher than those of mBMSCs on the Ti sample. These results indicated that the addition of macrophages could up-regulate the osteogenic gene expression levels of mBMSCs. However, the osteogenesis-related gene expression levels on Zn-Ti and Cu-Ti samples were still lower than those on the Ti sample. These results of osteogenic differentiation assays in mBMSCs were not consistent with previous studies, which reported that the implantation of Cu, Zn, and Ag ions could enhance the osteogenic differentiation compared with Ti. However, it was worth noting that in most cases, copper concentration (> 50 μM $\approx$ 3.2 ppm) and zinc concentration (> 10 μM $\approx$ 0.65 ppm) used in the previous experiments were much higher than its normal biological levels in the body [17,55,56]. Li et al. demonstrated that a copper concentration of 5 μM (0.32 ppm) added in the culture medium, resulted in the inhibition of osteogenesis of rBMSCs and the reduction of the osteogenic gene expression as well as the ALP activity both *in vitro* and *in vivo* tests [17]. Masako Ikeuchi's work showed that there was a species-dependent effect on the differentiation of stem cells at the same Zn concentration, the ALP activity of rBMSCs was higher than that of human MSCs [55]. These reports may explain the results that the osteogenic differentiation assays in mBMSCs were not consistent with the previous work. Also, the difference in cell species and preparation parameters of samples, including the implantation instruments, parameters, and environment, used in the experiments resulted in the various biological effects of ion-implanted samples.

3.4. In vivo studies of the immune response

The immune response of various samples *in vivo* was studied by using a mouse air-pouch model as described in the animal experiment. The histological observation was taken at postoperative days 1 and 4 and air-pouch tissue sections were stained with HE and Masson's trichrome. HE and Masson's trichrome staining results (Fig. 5) showed that fibrous layers formed around the samples after implanted for 1 and 4 d (as indicated by the black arrows), containing a large number of inflammatory cells, including neutrophils and macrophages. The number of infiltrated inflammatory cells and the thickness of the fibrous layer around all samples on day 4 were decreased from those on day 1. The number of infiltrated inflammatory cells and the thickness of the fibrous layer on days 1 and 4 throughout PIII samples were less and thinner compared with those around the Ti sample. The quantitative analysis illustrated that both the number of infiltrated inflammatory cells and the thickness of the fibrous layer after implanted for 1 and 4 d around the Ag-Ti sample were the least and the thinnest among the four group samples. The number of inflammatory cells and the thickness of fibrous layers were as the following trend: Ag-Ti < Zn-Ti < Cu-Ti < Ti, which was in agreement with the *in vitro* results. These results may benefit from the ability of the Ag-Ti sample, which could significantly promote the polarization of M2 macrophages and control the M1 macrophage polarization, further inhibit the fibrous capsule formation and the infiltration of inflammatory cells [57].

4. Discussion

Three different ds-block elements were introduced on a titanium substrate using the PIII method in this work. The high-resolution spectral results of the sample surfaces tested by XPS were demonstrated that three metal ions were indeed implanted onto the titanium substrate (Fig. 1c) and the contents of the implantation ions on the surfaces of PIII samples were very close (Table S5). Furthermore, the XPS results indicated that the main existing forms of the three ds-block elements on the titanium surface are CuO, ZnO, and Ag, respectively. The different oxidation valence states of the three PIII ds-block elements on the titanium surface are attributed to the different standard electrode potentials of Ti (E°_{Ti}), Zn (E°_{Zn}), Cu (E°_{Cu}), and Ag (E°_{Ag}), which are −1.630 V, −0.7618 V, +0.3400 V and +0.7996 V, respectively. The trend of the losing electron ability of the ds-block elements on titanium surface is as follows: Zn > Cu > Ag, while the trend of oxidation of the corresponding cation is opposite: $Ag^{+} > Cu^{2+} > Zn^{2+}$ [58]. The

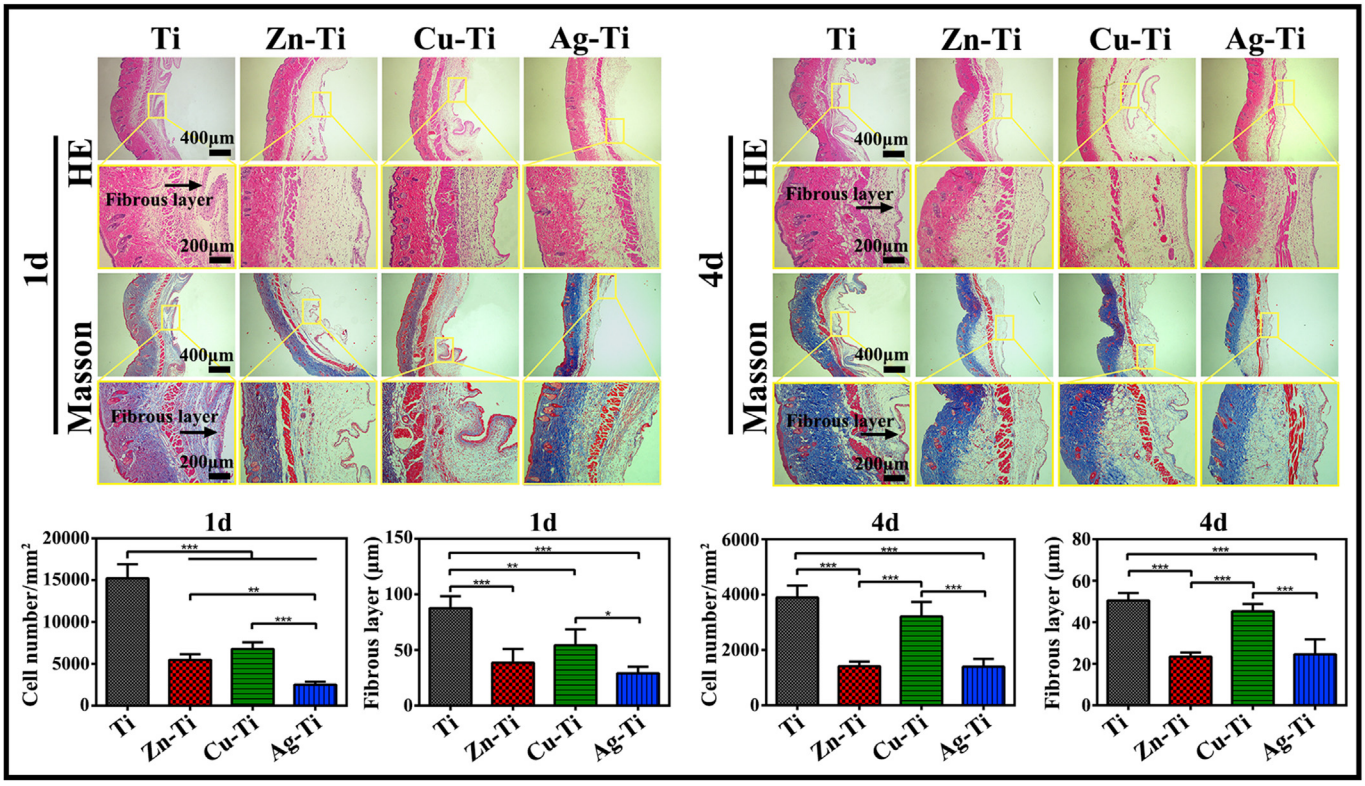

Fig. 5. The immune response of macrophages on various samples *in vivo*. Images of hematoxylin-eosin (HE) staining and Masson's trichrome staining of air-pouch tissues adjacent to different samples at 1 and 4 d after implantation. Images of HE staining of tissues showing the entire structure and layers of the air-pouch tissues and images of Masson's trichrome-stained tissues displaying the fibrous tissues and the infiltrating cells on day 1 and 4. The corresponding thickness of the fibrous layers and the number of infiltrated cells on day 1 and 4.

electrode potential of Ag is the highest among the four metal ions, the electrons of titanium would be prone to transfer to sliver and Ag^+ is easily reduced to Ag. So instead of forming an oxide film like zinc and copper, silver on titanium surface forms metal nanoparticles (Fig. 1a). Their different oxidation valence states further influenced the electrochemical properties of sample surfaces, including zeta potentials and corrosion resistance of the PIII samples (Figs. S3–S5).

All PIII samples could slowly release the metal ions in the PBS solution and the released amounts of ions were very similar ($\sim 10^{-1}$ ppm) (Fig. 1d). Although the previous studies had reported that free metallic ions exhibited cytotoxicity, the cell experiments in this work showed that the PIII samples possessed good bio-compatibility with both macrophages and mBMSCs (Figs. S6 and S12). Since the type of released metal ions from the three PIII samples were completely different, it is not surprising to find that the various ds-block element introduced titanium surfaces have discriminative effects on regulating cell response of both immune cells (macrophages) and osteoblasts (mBMSCs).

Titanium and PIII samples, without antigenicity, could not induce acquired immune response, thus it is focused on the host innate immune response caused by implanted biomaterials in this work [26,59]. Macrophages, as the innate immune cells, with plastic phenotypes and functions play an important role in inflammation and tissue repair caused by various diseases and trauma. They are divided into two major phenotypes under the stimulus of implants, the classical activated M1 phenotype and the alternatively activated M2 phenotype [60,61]. M1 phenotype macrophages could secrete inflammatory cytokines and increase the synthesis of ROS and nitrogen free radicals to be a key part of the host defense mechanism [48,49]. M2 phenotype macrophages (M2a, M2b, M2c, and M2d) could over-express IL-10 and other anti-inflammatory cytokines to limit the inflammation as well as suppress the immune response and secrete cytokines to participate in the repair of bone and other tissues [60,61]. It is important to effectively and timely regulate the polarization of M1 macrophages and induce M2 macrophages to release osteogenesis-related cytokines, which is conducive to promote the combination of materials and bone tissues [28,62]. All PIII samples could promote the polarization of macrophages and increase the polarization ratio of M2/M1 compared with the Ti sample. The M2/M1 polarization ratio of macrophages on the three PIII samples exerted the following trend: Ag-Ti > Zn-Ti > Cu-Ti > Ti, which was as the same trend of the corresponding anti-inflammatory response of macrophages on sample surfaces. The *in vivo* experiment results also revealed that the number of infiltrating cells and the thickness of the fibrous layer around the PIII samples were lower and thinner compared with the Ti sample both at 1 and 4 d. The anti-inflammatory response of immune cells on around the implanted samples showed the same following trend as *in vitro*: Ag-Ti > Zn-Ti > Cu-Ti > Ti.

The mBMSCs possess the potential to differentiate into bone cells and are used to evaluate the osteogenic activity of samples [63]. The staining and quantitative results of ALP expression, collagen secretion, and ECM mineralization were shown that there was no difference in osteogenic differentiation of mBMSCs cultured alone among the four group samples. The PCR results exerted that the PIII samples down-regulated the expressions of osteogenic genes in mBMSCs cultured alone compared with the Ti sample. The osteogenic gene expression levels of mBMSCs on the Ag-Ti sample were the highest among the three PIII samples.

When macrophages and mBMSCs were co-cultured directly on the sample surface *in vitro*, the general trend of the anti-inflammatory response of macrophages on sample surfaces was as follows: Ag-Ti > Zn-Ti > Cu-Ti > Ti. The osteogenic differentiation of mBMSCs on PIII samples was better than that of cells on the Ti sample, especially that of cells on the Ag-Ti sample. The osteogenic activity of mBMSCs on the PIII sample surface showed the following trend: Ag-Ti > Zn-Ti > Cu-

Ti. The results of the immune response of macrophages on various samples *in vivo* were in agreement with the results of *in vitro* experiments. PIII samples could reduce the inflammation and enhance the anti-inflammation. Ag-Ti sample exhibited the best regulation of improving anti-inflammatory response, followed by the Zn-Ti sample. This is an interesting result that it is generally believed that zinc and copper have better osteogenesis and immune regulation than silver in the previous literature. Because that both copper and zinc are key trace elements in the body and act as messengers in a series of biological reactions, while silver is generally considered as a toxic element [20,23,55]. More specifically, Cu participates in the synthesis of copper-containing superoxide dismutase, cytochrome oxidase, and lysyl oxidase, all of which could reduce oxidative damage by altering inflammation. For instance, copper/zinc superoxide dismutase (Cu/Zn SOD), an endogenous antioxidant in cells, could prevent the automatic oxidation and decrease the release of ferrous ion in injury tissues. [64–66]. Zinc acts as a second messenger to regulate the intracellular signaling cascades and alters the ligand-receptor binding by changing the affinity of the ligands or receptors. Meanwhile, Zn also could affect the generation and stability of cell membrane complexes with causing the receptors assembled or disassembled as well as altering their endocytosis [67–69]. Zn would activate MAPK in immune cells, stabilize MyD88 expression level, alter the polarization of M1/M2 by inhibiting the activity of STAT6 in macrophages and change Irt-like proteins (Zip) and Zn transporter (ZnT) family expression in DCs and T cells. Another important zinc-finger protein A20 (also called as TNFAIP3) in immune cells could inhibit NF-κB activity and TNF-mediated programmed cell death (PCD) in the TNF-receptor (TNFR) and toll-like receptor (TLR) pathways [70,71]. It is widely assumed that both Ag NPs and free Ag show obvious cytotoxicity to cells and promote cell apoptosis through oxidative stress [72,73]. Ag NPs, which are phagocytized by cells, stimulate immune cells to produce a large amount of ROS and improve the activation of the NF-κB signaling pathway to up-regulate inflammatory responses [74]. Free Ag combines with a variety of biomolecules in cells, including nucleic acids, cell wall components, –SH of metabolic enzymes, to inhibit the mitochondrial functions and cause the disorder of cell energy metabolism, further leading to cell death [72].

These unconventional results may be due to the different existing forms of the three ds-block elements. The biochemistry of the element much depends on its valence electronic structure [9,15]. These three elements, Cu, Zn, and Ag, are belonging to ds-block elements and possess similar valence electronic structures (n-1) $d^{10}ns^{1-2}$. However, as analyzed above, due to their different Fermi energy level, the implanted ions, Cu, Zn, and Ag, on the titanium surface are in the form of CuO (Cu^{2+}), ZnO (Zn^{2+}), and Ag, respectively. The sketch map of the electronic configurations of the ds-block elements when they gain and lose electrons on the titanium substrate is shown in Fig. 6. The implanted copper lost its outermost electron ($4s^1$) and a 3d-block electron ($3d^1$) to form a steady-state Cu^{2+} ($3d^9$), the number of valence electrons of Cu^{2+} was 9. The implanted zinc tended to lose two electrons in its outermost electron shell ($4s^2$) and was oxidized to Zn^{2+} ($3d^{10}$), the number of valence electrons of Zn^{2+} was 10. Because silver had a large number of positive charges, its nuclear possessed a strong binding ability to surrounding electrons. As a result of the penetration effect, it was not easy for Ag to lose its valence electrons ($4d^{10}5s^1$) and Ag^+ was also easily reduced to metal Ag ($4d^{10}5s^1$), the number of valence electrons of Ag was still 11. So, based on their nuclear charges and the configurations of extranuclear electrons, the implanted Zn, Cu, and Ag ions on the Ti substrate were in the form of Zn^{2+}, Cu^{2+}, and Ag, respectively. The number of valence electrons of Zn^{2+}, Cu^{2+} and Ag on Ti substrate showed the following trend: Ag > Zn^{2+} > Cu^{2+}. The number of valence electrons of an element is related to its redox ability. Ag^+ possesses the strongest oxidation property among the three ds-block elements and is easily reduced to Ag, then followed by Cu^{2+} with the lowest electron number in the valence orbital ($3\ d^9$), which is more liable to gain electrons from Ti ($3d^24s^2$) than Zn^{2+}. Zn^{2+} exhibits the lowest oxidation property. Comparing with the results of biological experiments, it can be found that the osteogenesis and immune regulation of the PIII samples are significantly related to the number of valence electrons of the implanted ions, which were in the steady states on the Ti substrate. As the number of valence electrons increases, the oxidizing capacity of the introduced ds-block element increases, and its biological properties including osteogenic activity and anti-inflammatory response are optimized.

To confirm the viewpoints above, the activation of PGE2-related signaling pathways were tested in this work, which is associated with oxidative stress (Fig. 7). The inflammatory response induced by both the surgery and implant biomaterials can lead to an excessive reactive oxygen species (ROS) in the body, which is beyond the body's antioxidant defense system, that is, oxidative stress occurs at the implant site [25,26]. The produced ROS can act as a second messenger to regulate the signal transduction and cellular gene expression [75]. Previous studies have reported that ROS can up-regulate the expression of cyclooxygenase-2 (COX-2), which promotes the transformation of arachidonic acid (AA) into PGE2 and mediates the physiological responses in the body, including the immune response and osteogenesis. For example, ROS can improve the expression of COX-2 in renal and respiratory epithelial tissues [76]. Liu et al. also found that ROS, COX-2, and PGE2 levels increased with the UVB-mediated ketoprofen (KP) concentration arising in the pre-treated human keratinocyte cell KC with UVB-mediated KP, but when cells were pre-treated with ROS inhibition, ROS level reduced with a decrease in COX-2/PGE2 levels [77]. PGE2 and PGI2, PGF2α, PGD2, thromboxane (TxA2) belong to prostaglandin (PG), a kind of lipid medium, produced by the enzymatic metabolism of AA [78]. All kinds of cells in the body could secrete prostaglandin, the synthesized prostaglandin was released to the extracellular cells rapidly due to its short half-life and the best detection method of PGE2 is by using ELISA [79]. As shown in Fig. 7, PGE2 binds to four specific receptors (G Protein-Coupled Receptors, GPCRs) EP1-EP4 to achieve its biological activity [78]. Also, EP2 and EP4 receptors are related to bone formation [78]. By coupling with the activated G proteins (Gs), EP2 and EP4 can increase the production of intracellular cAMP to activate protein kinase A (PKA), PI3K, and AKT. Then, they subsequently activate the downstream molecules (such as CREB, ERK, and NF-κB) in the PGE2-cAMP signal transduction pathway. And they further induce osteogenic differentiation and decrease the inflammation via promoting the polarization of M2 phenotype macrophages and the release of anti-inflammatory cytokines [80]. It is noticed that there is a positive feedback between PGE2 and the rate-limiting enzyme COX-2 in its synthesis process.

ROS levels of macrophages cultured alone on the sample's surface were shown in Fig. 8a. Ag-Ti sample can induce macrophages to produce the most ROS among the three PIII samples based on the strongest oxidation activity of Ag^+. Although the oxidability of Cu^{2+} is stronger than that of Zn^{2+}, Cu^{2+} participates in the synthesis of various reducible metal complex enzymes, such as ceruloplasmin, lysyl oxidase, and superoxide dismutase, to remove ROS in cells. The intracellular ROS content of cells on the Cu-Ti sample was lower than that of cells on the Zn-Ti sample. Because ROS could enhance the expression of COX-2, further promote the synthesis and release of PGE2, which was confirmed by the increase in the gene expression level of PGI_2 (another type of PG) (Fig. 8b and c). Thus, the amount of PGE2 released by macrophages on the sample surface is in direct proportion to the intracellular ROS level, which is as the following trend: Ag-Ti > Zn-Ti > Cu-Ti > Ti (Fig. 8a). Under the action of cellular autocrine and paracrine, the increase of PGE2 level improves the activity of its membrane receptors EP2 and EP4, up-regulates the expression levels of the downstream genes (cAMP and CREB), and promotes macrophages to polarize towards M2 phenotype with releasing anti-inflammatory factors. Meanwhile, the increase of PGE2 level can also down-regulate the expression level of inflammatory genes in the NF-κB signaling pathway ulteriorly (Fig. 8b). Therefore, the sample which can stimulate

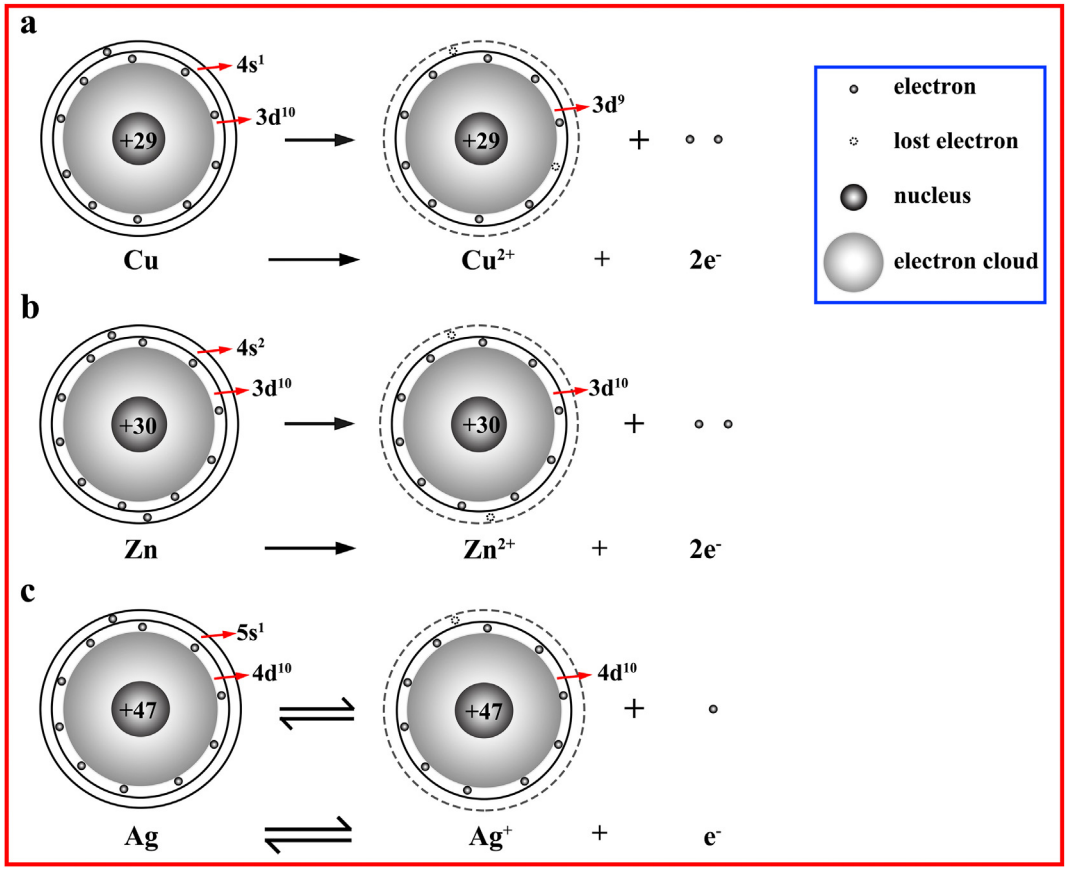

Fig. 6. The schematic diagram of the configurations of extra-nuclear electrons of ds-block elements when they gain and lose electrons on the titanium substrate.

macrophages to produce plenty of ROS exerts a strong anti-inflammatory effect, while the sample with a low ROS level in macrophages exerts a weak anti-inflammatory effect (Fig. 3). Moreover, the anti-inflammatory effect of the ds-block element is enhanced with the increase of the number of valence electrons: Ag-Ti > Zn-Ti > Cu-Ti > Ti.

When macrophages and mBMSCs were directly co-cultured, both of them could secret PGE2 and the PGE2 levels of all samples in the co-cultural medium increased (Fig. 8a). PGE2 secreted by mBMSCs on sample surfaces acted on macrophages through paracrine action. It led to the expression levels of cell membrane receptors genes (EP2 and EP4) as well as the downstream genes cAMP and CREB in macrophages on sample surfaces significantly increasing (Fig. 8b). It further promoted the co-cultured macrophages on sample surfaces to polarize towards M2 phenotype, enhanced the anti-inflammatory effect of macrophages on samples (Figs. 2 and 3). The anti-inflammatory effect of cells in co-culture condition on sample surfaces was as the same trend of the amounts of PGE2: Ag-Ti > Zn-Ti > Cu-Ti > Ti. Similarly, as shown in Fig. 8c, PGE2 secreted by macrophages could also act on mBMSCs in a paracrine manner and up-regulate the expression levels of the membrane receptors (EP2 and EP4). Meanwhile, it up-regulated the expression levels of the downstream gene cAMP and COX-2 in the co-cultured mBMSCs on sample surfaces, further promote the osteogenic differentiation of mBMSCs (Fig. 4). Besides, M2 macrophages could promote the osteogenic differentiation of the co-cultured mBMSCs by secreting cytokines, e.g. TGF-β and IL-10 (Fig. 3a). The acceleration in the osteogenic differentiation of mBMSCs was related to the polarization ratio of M2 macrophage on sample surfaces and the corresponding trend was Ag-Ti > Zn-Ti > Cu-Ti > Ti. Thus, in the co-culture condition, mBMSCs can promote macrophages to polarize into the M2 phenotype and enhance the anti-inflammatory effect of macrophages on sample surface through the paracrine action of PGE2 (Figs. 2, 3 and 8a). Macrophages can also up-regulate the gene expression level of cAMP and increase the osteogenic differentiation of mBMSCs through the PGE2 paracrine action (Figs. 4 and 8). It is worth noting that in the co-culture condition, the anti-inflammatory effect of macrophages and the osteogenic activity of mBMSCs on the PIII sample surface were in the same trend: Ag-Ti > Zn-Ti > Cu-Ti, which is correlated with the number of valence electrons of the introduced ds-block elements.

However, although it was concluded that the anti-inflammatory effect of the introduced elements in the ds-block was increased with the arising of the number of valence electrons, this rule was only concluded from the results of the pair-wise comparison between two elements in the same group or the same period. It was needed to further expand the elements in the ds-block, such as gold (Au) and cadmium (Cd), which could be introduced on the Ti substrate, to obtain a more universal result. Also, it was short of a good explanation for the root cause of the differences in biological effects caused by the different ds-block elements on the titanium substrate.

5. Conclusions

Three ds-block elements, Zn, Cu, and Ag, were introduced on the titanium surface by PIII method to investigate their immune response of macrophages, their osteogenic differentiation of mBMSCs, and further study the correlation between macrophages and mBMSCs on sample surfaces as well as the involved mechanisms. According to their outmost orbital structures, the implanted ions, Zn, Cu, and Ag, on the Ti substrate were in the form of Zn^{2+}, Cu^{2+}, and Ag. The number of valence electrons of ds-block elements was as the following trend: Ag-Ti > Zn-Ti > Cu-Ti. The results of immune responses of macrophages both in single-culture and co-culture conditions on sample surfaces showed that the implanted samples could up-regulate the anti-inflammation and down-regulate the inflammation compared with the Ti

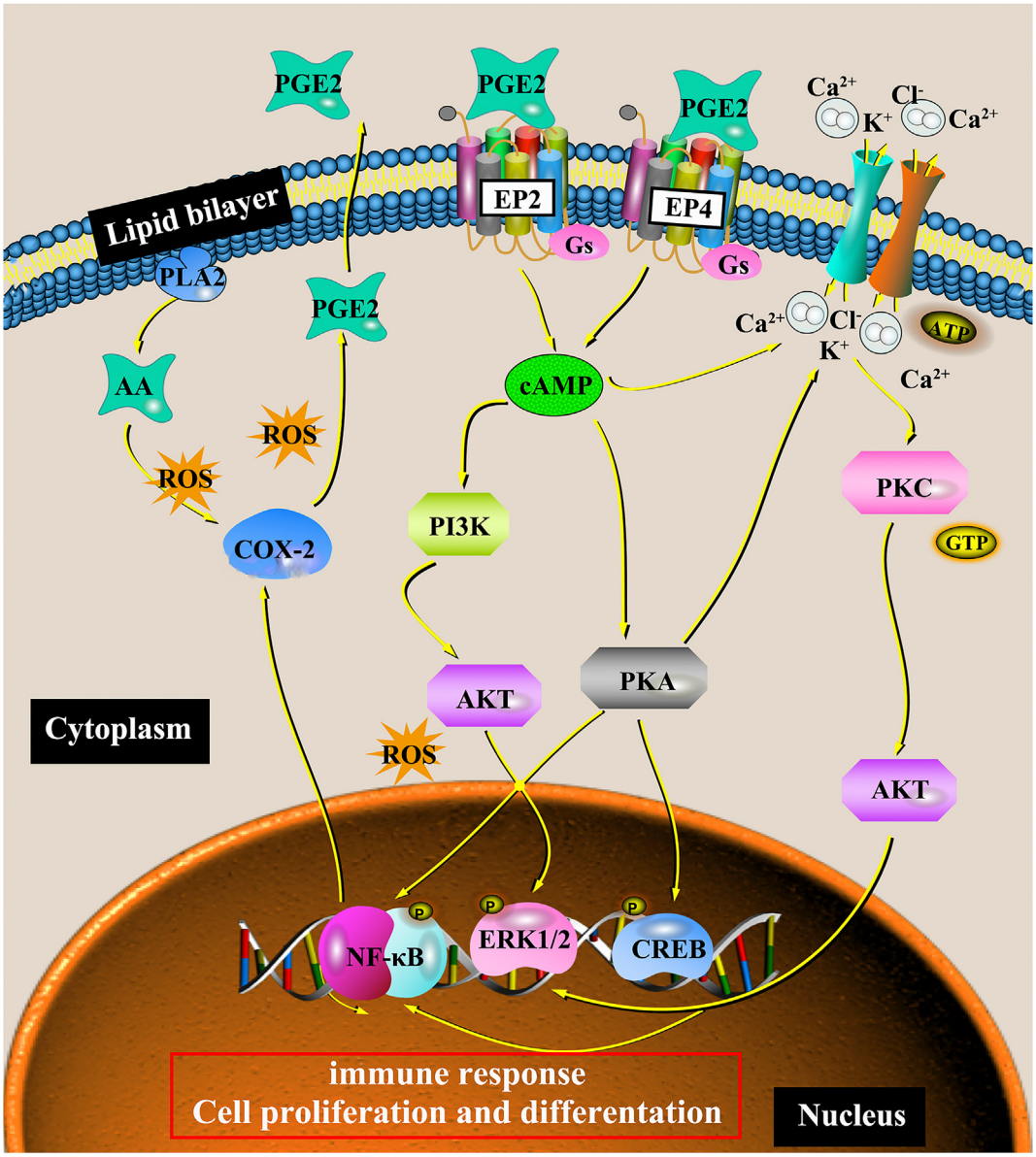

Fig. 7. The PGE2-related signaling pathway mediates the immune response of macrophages and the osteogenesis of mBMSCs cultured on sample surfaces in single-culture and co-culture conditions.

sample. With the number of valence electrons (Zn^{2+}, Cu^{2+}, and Ag) increasing, the anti-inflammatory effects of ds-block elements were enhanced through improving cellular ROS levels and boosting the activity of the PGE2-related signaling pathway. The trend of anti-inflammatory effects of macrophages on various samples showed as follow: Ag-Ti > Zn-Ti > Cu-Ti > Ti.

Macrophages and mBMSCs regulated each other's biological responses through the paracrine of PGE2. The addition of mBMSCs increased the PGE2 levels in the co-culture medium and promoted the anti-inflammatory response of macrophages on samples. The addition of macrophages also significantly enhanced the osteogenic differentiation of mBMSCs on samples by increasing the PGE2 levels in the co-culture medium. These results could be explained by the PGE2-related signaling pathway. This work provides a new sight into the selection of the ds-block elements to obtain the proper biological response in the design of the biomaterial surface.

Ethical approval

All animal experiments were approved and carried out in accordance to the Institutional Animal Care and Use Committee (SHRM-IACUC-016). No human subjective was involved in this experiment.

Date availability

The raw/processed data required to reproduce these findings cannot be shared at this time as the data also forms part of an ongoing study. However, they can be provided upon request.

CRediT authorship contribution statement

Lan Chen: Conceptualization, Methodology, Software, Writing - original draft, Visualization. **Donghui Wang:** Data curation, Writing - review & editing, Funding acquisition. **Jiajun Qiu:** Writing - review & editing, Investigation, Resources. **Xianming Zhang:** Writing - review & editing, Investigation, Resources. **Xingdan Liu:** Writing - review &

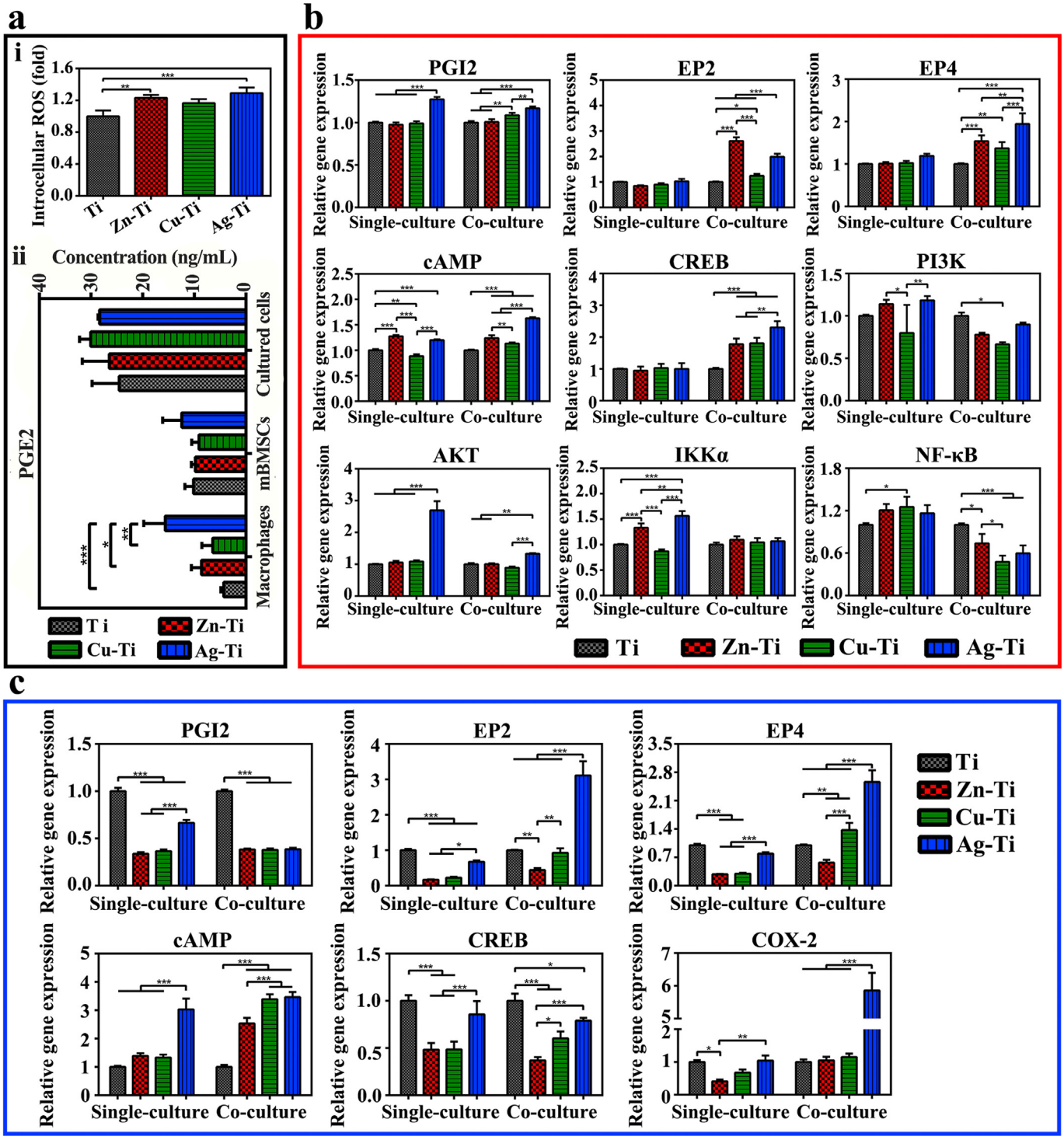

Fig. 8. Cytokine secretion and gene expression levels in PGE2-related signaling pathway in macrophages and mBMSCs on various samples *in vitro*. (a) Intracellular ROS levels of macrophages on day 4 (i); ELISA determinations of PGE2 cytokine secreted from macrophages and mBMSCs in single-culture and co-culture conditions cultured on samples for 4 and 10 d, respectively (ii). (b) PCR results of PGE2-related gene levels in macrophages in single-culture and co-culture conditions on day 4 after cultured on different samples. (c) PCR results of PGE2-related gene levels in mBMSCs in single-culture and co-culture conditions on day 10 after cultured on different samples.

editing, Investigation, Resources. **Yuqin Qiao:** Writing - review & editing, Funding acquisition. **Xuanyong Liu:** Writing - review & editing, Project administration, Supervision, Funding acquisition.

Declaration of competing interests

The authors declare that they have no known competing financial interests or personal relationships that could have appeared to influence the work reported in this paper.

Acknowledgments

This work was financially supported by the National Natural Science Foundation of China (51831011 and 31570973), National Science Foundation for Distinguished Young Scholars of China (51525207), Science and Technology Commission of Shanghai Municipality (19JC1415500, 17441904000, and 18YF1426900) are acknowledged. The authors are very grateful to the SEM support provided by *Chucheng Lin* (The Analysis and Testing Center for Inorganic Materials, Shanghai Institute of Ceramics, Chinese Academy of Sciences).

Appendix A. Supplementary data

Supplementary data to this article can be found online at https://doi.org/10.1016/j.bioactmat.2020.08.001.

References

[1] C. Santini, M. Pellei, V. Gandin, M. Porchia, F. Tisato, C. Marzano, Advances in copper complexes as anticancer agents, Chem. Rev. 114 (1) (2014) 815–862.
[2] R. Rinaldi, A. Biasco, G. Maruccio, R. Cingolani, D. Alliata, L. Andolfi, P. Facci, F. De Rienzo, R. Di Felice, E. Molinari, Solid-state molecular rectifier based on self-organized metalloproteins, Adv. Mater. 14 (20) (2002) 1453–1457.
[3] Y. Wang, T.X. Chen, Z.T. Zhang, Y.N. Ni, Cytidine-stabilized copper nanoclusters as a fluorescent probe for sensing of copper ions and hemin, RSC Adv. 8 (17) (2018) 9057–9062.
[4] C.C. Huang, Z. Yang, K.H. Lee, H.T. Chang, Synthesis of highly fluorescent gold nanoparticles for sensing Mercury(II), Angew. Chem. Int. Ed. 46 (36) (2007) 6824–6828.
[5] M. Kang, S. Jung, H.N. Zhang, T. Kang, H. Kang, Y. Yoo, J.P. Hong, J.P. Ahn, J. Kwak, D. Jeon, N.A. Kotov, B. Kim, Subcellular neural probes from single-crystal gold nanowires, ACS Nano 8 (8) (2014) 8182–8189.
[6] K. Critchley, B.P. Khanal, M.L. Gorzny, L. Vigderman, S.D. Evans, E.R. Zubarev, N.A. Kotov, Near-bulk conductivity of gold nanowires as nanoscale interconnects and the role of atomically smooth interface, Adv. Mater. 22 (21) (2010) 2338–2342.
[7] R.C. Lin, C.J. Deng, X.X. Li, Y.Q. Liu, M. Zhang, C. Qin, Q.Q. Yao, L.M. Wang, C.T. Wu, Copper-incorporated bioactive glass-ceramics inducing anti-inflammatory phenotype and regeneration of cartilage/bone interface, Theranostics 9 (21) (2019) 6300–6313.
[8] Y.Q. Qiao, W.J. Zhang, P. Tian, F.H. Meng, H.Q. Zhu, X.Q. Jiang, X.Y. Liu, P.K. Chu, Stimulation of bone growth following zinc incorporation into biomaterials, Biomaterials 35 (25) (2014) 6882–6897.
[9] H.L. Cao, W.J. Zhang, F.H. Meng, J.S. Guo, D.H. Wang, S. Qian, X.Q. Jiang, X.Y. Liu, P.K. Chu, Osteogenesis catalyzed by titanium-supported silver nanoparticles, ACS Appl. Mater. Interfaces 9 (6) (2017) 5149–5157.
[10] Z.Q. Xu, M. Li, X. Li, X.M. Liu, F. Ma, S.L. Wu, K.W.K. Yeung, Y. Han, P.K. Chu, Antibacterial activity of silver doped titanate nanowires on Ti implants, ACS Appl. Mater. Interfaces 8 (26) (2016) 16584–16594.
[11] W. Yu, T.W. Sun, C. Qi, Z. Ding, H. Zhao, S. Zhao, Z. Shi, Y.J. Zhu, D. Chen, Y. He, Evaluation of zinc-doped mesoporous hydroxyapatite microspheres for the construction of a novel biomimetic scaffold optimized for bone augmentation, Int. J. Nanomed. 12 (2017) 2293–2306.
[12] Y.C. Zhao, H.L. Cao, H. Qin, T. Cheng, S. Qian, M.Q. Cheng, X.C. Peng, J.X. Wang, Y. Zhang, G.D. Jin, X.L. Zhang, X.Y. Liu, P.K. Chu, Balancing the osteogenic and antibacterial properties of titanium by codoping of Mg and Ag: an in vitro and in vivo study, ACS Appl. Mater. Interfaces 7 (32) (2015) 17826–17836.
[13] G.D. Jin, H. Qin, H.L. Cao, S. Qian, Y.C. Zhao, X.C. Peng, X.L. Zhang, X.Y. Liu, P.K. Chu, Synergistic effects of dual Zn/Ag ion implantation in osteogenic activity and antibacterial ability of titanium, Biomaterials 35 (27) (2014) 7699–7713.
[14] K. Huo, N. Xu, J. Fu, P. Chu, Bioactive inorganic-ion-doped titania nanotube coatings on bone implants with enhanced osteogenic activity and antibacterial properties, in: K. Subramani, Waqar Ahmed (Eds.), Nanobiomaterials in Clinical Dentistry, 2019, pp. 401–427.
[15] G.D. Jin, H. Qin, H.L. Cao, Y.Q. Qiao, Y.C. Zhao, X.C. Peng, X.L. Zhang, X.Y. Liu, P.K. Chu, Zn/Ag micro-galvanic couples formed on titanium and osseointegration effects in the presence of S-aureus, Biomaterials 65 (2015) 22–31.
[16] I. Burghardt, F. Lüthen, C. Prinz, B. Kreikemeyer, C. Zietz, H.-G. Neumann, J. Rychly, A dual function of copper in designing regenerative implants, Biomaterials 44 (2015) 36–44.
[17] S. Li, M. Wang, X. Chen, S.F. Li, J. Li-Ling, H.Q. Xie, Inhibition of osteogenic differentiation of mesenchymal stem cells by copper supplementation, Cell Prolif 47 (1) (2014) 81–90.
[18] L. Yang, S. Perez-Amodio, F.Y.F. Barrère-de Groot, V. Everts, C.A. van Blitterswijk, P. Habibovic, The effects of inorganic additives to calcium phosphate on in vitro behavior of osteoblasts and osteoclasts, Biomaterials 31 (11) (2010) 2976–2989.
[19] W. He, Y. Zheng, Q. Feng, T.A. Elkhooly, X. Liu, X. Yang, Y. Wang, Y. Xie, Silver nanoparticles stimulate osteogenesis of human mesenchymal stem cells through activation of autophagy, Nanomedicine 15 (4) (2020) 337–353.
[20] H.T. Ratte, Bioaccumulation and toxicity of silver compounds: a review, Environ. Toxicol. Chem. 18 (1) (1999) 89–108.
[21] X.D. Zhang, D. Wu, X. Shen, P.X. Liu, F.Y. Fan, S.J. Fan, Vivo renal clearance, biodistribution, toxicity of gold nanoclusters, Biomaterials 33 (18) (2012) 4628–4638.
[22] J.E.J. Li, N. Kawazoe, G. Chen, Gold nanoparticles with different charge and moiety induce differential cell response on mesenchymal stem cell osteogenesis, Biomaterials 54 (2015) 226–236.
[23] C.E. Albers, W. Hofstetter, K.A. Siebenrock, R. Landmann, F.M. Klenke, In vitro cytotoxicity of silver nanoparticles on osteoblasts and osteoclasts at antibacterial concentrations, Nanotoxicology 7 (1) (2013) 30–36.
[24] S.E. Rossiter, M.H. Fletcher, W.M. Wuest, Natural products as platforms to overcome antibiotic resistance, Chem. Rev. 117 (19) (2017) 12415–12474.
[25] D.M. Vasconcelos, S.G. Santos, M. Lamghari, M.A. Barbosa, The two faces of metal ions: from implants rejection to tissue repair/regeneration, Biomaterials 84 (2016) 262–275.
[26] S. Franz, S. Rammelt, D. Scharnweber, J.C. Simon, Immune responses to implants – a review of the implications for the design of immunomodulatory biomaterials, Biomaterials 32 (28) (2011) 6692–6709.
[27] M.B. Gorbet, M.V. Sefton, Biomaterial-associated thrombosis: roles of coagulation factors, complement, platelets and leukocytes, Biomaterials 25 (26) (2004) 5681–5703.
[28] Z. Chen, T. Klein, R.Z. Murray, R. Crawford, J. Chang, C. Wu, Y. Xiao, Osteoimmunomodulation for the development of advanced bone biomaterials, Mater. Today 19 (6) (2016) 304–321.
[29] J. He, G. Chen, M. Liu, Z. Xu, H. Chen, L. Yang, Y. Lv, Scaffold strategies for modulating immune microenvironment during bone regeneration, Mater. Sci. Eng. C 108 (2020) 110411–110426.
[30] H. Feng, G. Wang, G. Wu, W. Jin, H. Wu, P.K. Chu, Plasma and ion-beam modification of metallic biomaterials for improved anti-bacterial properties, Surf. Coating. Technol. 306 (2016) 140–146.
[31] M. Cheng, Y. Qiao, Q. Wang, H. Qin, X. Zhang, X. Liu, Dual ions implantation of zirconium and nitrogen into magnesium alloys for enhanced corrosion resistance, antimicrobial activity and biocompatibility, Colloids Surf. B Biointerfaces 148 (2016) 200–210.
[32] L. Zheng, S. Qian, X. Liu, Enhanced osteogenic activity and bacteriostatic effect of TiO2 coatings via hydrogen ion implantation, Mater. Lett. 253 (2019) 95–98.
[33] G.D. Jin, H.L. Cao, Y.Q. Qiao, F.H. Meng, H.Q. Zhu, X.Y. Liu, Osteogenic activity and antibacterial effect of zinc ion implanted titanium, Colloids Surf. B Biointerfaces 117 (2014) 158–165.
[34] H. Cao, X. Liu, F. Meng, P.K. Chu, Biological actions of silver nanoparticles embedded in titanium controlled by micro-galvanic effects, Biomaterials 32 (3) (2011) 693–705.
[35] G. Jin, L. Ouyang, D. Wang, Y. Qiao, X. Liu, Antibacterial activity, osteogenic and angiogenic behaviors of copper-bearing titanium synthesized by PIII&D, J. Mater. Chem. B 4 (2016) 1296–1309.
[36] L. Chen, D. Wang, F. Peng, J. Qiu, L. Ouyang, Y. Qiao, X. Liu, Nanostructural surfaces with different elastic moduli regulate the immune response by stretching macrophages, Nano Lett. 19 (6) (2019) 3480–3489.
[37] J.J. Qiu, L. Liu, B.H. Chen, Y.Q. Qiao, H.L. Cao, H.Q. Zhu, X.Y. Liu, Graphene oxide as a dual Zn/Mg ion carrier and release platform: enhanced osteogenic activity and antibacterial properties, J. Math. Chem. B 6 (13) (2018) 2004–2012.
[38] B. Li, H. Cao, Y. Zhao, M. Cheng, H. Qin, T. Cheng, Y. Hu, X. Zhang, X. Liu, In vitro and in vivo responses of macrophages to magnesium-doped titanium, Sci. Rep. 7 (1) (2017) 42707–42719.
[39] D.P. Vasconcelos, M. Costa, I.F. Amaral, M.A. Barbosa, A.P. Águas, J.N. Barbosa, Development of an immunomodulatory biomaterial: using resolvin D1 to modulate inflammation, Biomaterials 53 (2015) 566–573.
[40] J. Fang, J. Zhao, Y. Sun, H. Ma, X. Yu, Y. Ma, Y. Ni, L. Zheng, Y. Zhou, Biocompatibility and antibacterial properties of zinc-ion implantation on titanium, J. Hard Tissue Biol. 23 (1) (2014) 35–44.
[41] M. Polak, A. Ohl, M. Quaas, G. Lukowski, F. Lüthen, K.-D. Weltmann, K. Schröder, Oxygen and water plasma-immersion ion implantation of copper into titanium for antibacterial surfaces of medical implants, Adv. Eng. Mater. 12 (9) (2010) B511–B518.
[42] B.R. Strohmeier, D.M. Hercules, Surface spectroscopic characterization of the interaction between zinc ions and γ-alumina, J. Catal. 86 (2) (1984) 266–279.
[43] A. Miller, Copper by XPS, Surf. Sci. Spectra 2 (1) (1993) 55–60.
[44] F. Parmigiani, G. Pacchioni, F. Illas, P.S. Bagus, Studies of the Cu-O bond in cupric oxide by X-ray photoelectron spectroscopy and ab initio electronic structure models, J. Electron. Spectrosc. Relat. Phenom. 59 (3) (1992) 255–269.
[45] J. Li, Y. Qiao, Z. Ding, X. Liu, Microstructure and properties of Ag/N dual ions implanted titanium, Surf. Coating. Technol. 205 (23) (2011) 5430–5436.
[46] D. Wang, Z. Lin, T. Wang, Z. Yao, M. Qin, S. Zheng, W. Lu, Where does the toxicity of metal oxide nanoparticles come from: the nanoparticles, the ions, or a combination of both? J. Hazard Mater. 308 (2016) 328–334.
[47] K. Girigoswami, Toxicity of Metal Oxide Nanoparticles, in: Q. Saquib, M. Faisal, A.A. Al-Khedhairy, A.A. Alatar (Eds.), Cellular and Molecular Toxicology of Nanoparticles, Springer International Publishing, Cham, 2018, pp. 99–122.
[48] J. Yang, Y. Zhu, D. Duan, P. Wang, Y. Xin, L. Bai, Y. Liu, Y. Xu, Enhanced activity of macrophage M1/M2 phenotypes in periodontitis, Arch. Oral Biol. 96 (2018) 234–242.
[49] V. Masola, G. Zaza, G. Bellin, L. Dall'Olmo, S. Granata, G. Vischini, M.F. Secchi, A. Lupo, G. Gambaro, M. Onisto, Heparanase regulates the M1 polarization of renal macrophages and their crosstalk with renal epithelial tubular cells after ischemia/reperfusion injury, Faseb. J. 32 (2) (2018) 742–756.
[50] A. Tan-Garcia, F. Lai, J.P.S. Yeong, S.E. Irac, P.Y. Ng, R. Msallam, J.C.T. Lim, L.-E. Wai, C.Y.L. Tham, S.P. Choo, T. Lim, D.Y. Young, R. D'Ambrosio, E. Degasperi,

R. Perbellini, E. Newell, N. Le Bert, F. Ginhoux, A. Bertoletti, Q. Chen, C.-A. Dutertre, Liver fibrosis and CD206+ macrophage accumulation are suppressed by anti-GM-CSF therapy, JHEP Reports 2 (1) (2020) 100062.
[51] T.H. Qazi, D.J. Mooney, G.N. Duda, S. Geissler, Biomaterials that promote cell-cell interactions enhance the paracrine function of MSCs, Biomaterials 140 (2017) 103–114.
[52] A. Buckels, Y. Zhang, J. Jiang, M. Athar, F. Afaq, L. Shevde-Samant, S.J. Frank, Autocrine/paracrine actions of growth hormone in human melanoma cell lines, Biochemistry and Biophysics Reports 21 (2020) 100716–100723.
[53] K. Sakaguchi, J.E. Herrera, S. Saito, T. Miki, M. Bustin, A. Vassilev, C.W. Anderson, E. Appella, DNA damage activates p53 through a phosphorylation-acetylation cascade, Genes Dev. 12 (18) (1998) 2831–2841.
[54] D. Kadosh, K. Struhl, Histone deacetylase activity of Rpd3 is important for transcriptional repression in vivo, Genes Dev. 12 (6) (1998) 797–805.
[55] M. Ikeuchi, A. Ito, Y. Dohi, H. Ohgushi, H. Shimaoka, K. Yonemasu, T. Tateishi, Osteogenic differentiation of cultured rat and human bone marrow cells on the surface of zinc-releasing calcium phosphate ceramics, J. Biomed. Mater. Res. 67A (4) (2003) 1115–1122.
[56] M. Yamaguchi, M. Hashizume, Effect of beta-alanyl-L-histidinato zinc on protein components in osteoblastic MC3T3-El cells: increase in osteocalcin, insulin-like growth factor-I and transforming growth factor-beta, Mol. Cell. Biochem. 136 (2) (1994) 163–169.
[57] X. Yuan, H. Cao, J. Wang, K. Tang, B. Li, Y. Zhao, M. Cheng, H. Qin, X. Liu, X. Zhang, Immunomodulatory effects of calcium and strontium Co-doped titanium oxides on osteogenesis, Front. Immunol. 8 (2017) 1196–1211.
[58] M.S. Antelman, F.J. Harris Jr., Electrochemical Series, in: M.S. Antelman, F.J. HarrisJr. (Eds.), The Encyclopedia of Chemical Electrode Potentials, Springer US, Boston, 1982, pp. 1–81.
[59] S.B. Goodman, Y.T. Konttinen, M. Takagi, Joint replacement surgery and the innate immune system, J. Long Term Eff. Med. Implants 24 (4) (2014) 253–257.
[60] A. Shapouri-Moghaddam, S. Mohammadian, H. Vazini, M. Taghadosi, S.-A. Esmaeili, F. Mardani, B. Seifi, A. Mohammadi, J.T. Afshari, A. Sahebkar, Macrophage plasticity, polarization, and function in health and disease, J. Cell. Physiol. 233 (9) (2018) 6425–6440.
[61] S.C. Funes, M. Rios, J. Escobar-Vera, A.M. Kalergis, Implications of macrophage polarization in autoimmunity, Immunology 154 (2) (2018) 186–195.
[62] R. Trindade, T. Albrektsson, S. Galli, Z. Prgomet, P. Tengvall, A. Wennerberg, Osseointegration and foreign body reaction: titanium implants activate the immune system and suppress bone resorption during the first 4 weeks after implantation, Clin. Implant Dent. Relat. Res. 20 (1) (2018) 82–91.
[63] Arnold I. Caplan, D. Correa, The MSC: an injury drugstore, Cell Stem Cell 9 (1) (2011) 11–15.
[64] S.S. Percival, Copper and immunity, Am. J. Clin. Nutr. 67 (5) (1998) 1064S–1068S.
[65] M.A. Saghiri, A. Asatourian, J. Orangi, C.M. Sorenson, N. Sheibani, Functional role of inorganic trace elements in angiogenesis—Part II: Cr, Si, Zn, Cu, and S, Crit. Rev. Oncol. Hematol. 96 (1) (2015) 143–155.
[66] M. Arredondo, M.T. Núñez, Iron and copper metabolism, Mol. Aspect. Med. 26 (4) (2005) 313–327.
[67] T. Hirano, M. Murakami, T. Fukada, K. Nishida, S. Yamasaki, T. Suzuki, Roles of Zinc and Zinc Signaling in Immunity: Zinc as an Intracellular Signaling Molecule, in: K.F. Austen, T. Honjo (Eds.), Advances in Immunology, Academic Press, New York, 2008, pp. 149–176.
[68] M. Maywald, I. Wessels, L. Rink, Zinc signals and immunity, Int. J. Mol. Sci., 18 (10) 2017 2222-2256.
[69] P. Bonaventura, G. Benedetti, F. Albarède, P. Miossec, Zinc and its role in immunity and inflammation, Autoimmun. Rev. 14 (4) (2015) 277–285.
[70] N. Shembade, A. Ma, E.W. Harhaj, Inhibition of NF-κB signaling by A20 through disruption of ubiquitin enzyme complexes, Science 327 (5969) (2010) 1135.
[71] E.G. Lee, D.L. Boone, S. Chai, S.L. Libby, M. Chien, J.P. Lodolce, A. Ma, Failure to regulate TNF-induced NF-κB and cell death responses in A20-deficient mice, Science 289 (5488) (2000) 2350.
[72] S. Juling, L. Böhmert, D. Lichtenstein, A. Oberemm, O. Creutzenberg, A.F. Thünemann, A. Braeuning, A. Lampen, Comparative proteomic analysis of hepatic effects induced by nanosilver, silver ions and nanoparticle coating in rats, Food Chem. Toxicol. 113 (2018) 255–266.
[73] C. Sun, N. Yin, R. Wen, W. Liu, Y. Jia, L. Hu, Q. Zhou, G. Jiang, Silver nanoparticles induced neurotoxicity through oxidative stress in rat cerebral astrocytes is distinct from the effects of silver ions, Neurotoxicology 52 (2016) 210–221.
[74] J. Shi, X. Sun, Y. Lin, X. Zou, Z. Li, Y. Liao, M. Du, H. Zhang, Endothelial cell injury and dysfunction induced by silver nanoparticles through oxidative stress via IKK/NF-κB pathways, Biomaterials 35 (24) (2014) 6657–6666.
[75] E. Rendra, V. Riabov, D.M. Mossel, T. Sevastyanova, M.C. Harmsen, J. Kzhyshkowska, Reactive oxygen species (ROS) in macrophage activation and function in diabetes, Immunobiology 224 (2) (2019) 242–253.
[76] Y. Zhao, P.V. Usatyuk, I.A. Gorshkova, D. He, T. Wang, L. Moreno-Vinasco, A.S. Geyh, P.N. Breysse, J.M. Samet, E.W. Spannhake, J.G.N. Garcia, V. Natarajan, Regulation of COX-2 expression and IL-6 release by particulate matter in airway epithelial cells, Am. J. Respir. Cell Mol. Biol. 40 (1) (2009) 19–30.
[77] S. Liu, H. Mizu, H. Yamauchi, Photoinflammatory responses to UV-irradiated ketoprofen mediated by the induction of ROS generation, enhancement of cyclooxygenase-2 expression, and regulation of multiple signaling pathways, Free Radic. Biol. Med. 48 (6) (2010) 772–780.
[78] K. Kawahara, H. Hohjoh, T. Inazumi, S. Tsuchiya, Y. Sugimoto, Prostaglandin E2-induced inflammation: relevance of prostaglandin E receptors, Biochim. Biophys. Acta 1851 (4) (2015) 414–421.
[79] M. Hamberg, B. Samuelsson, On the metabolism of prostaglandins E1 and E2 in man, J. Biol. Chem. 246 (22) (1971) 6713–6721.
[80] B. Luan, Y.-S. Yoon, J. Le Lay, K.H. Kaestner, S. Hedrick, M. Montminy, CREB pathway links PGE2 signaling with macrophage polarization, Proc. Natl. Acad. Sci. Unit. States Am. 112 (51) (2015) 15642–15647.